Australian Government
Department of Defence
Defence Science and
Technology Organisation

Models of Land Clutter vs Grazing Angle, Spatial Distribution and Temporal Distribution - L-Band VV Polarisation Perspective

Yunhan Dong

DSTO-RR-0273

Australian Government
Department of Defence
Defence Science and
Technology Organisation

Models of Land Clutter vs Grazing Angle, Spatial Distribution and Temporal Distribution – L-Band VV Polarisation Perspective

Yunhan Dong

Electronic Warfare and Radar Division
Electronics and Surveillance Research Laboratory

DSTO-RR-0273

ABSTRACT

Land clutter issues and modelling from a perspective of L-band VV polarisation are addressed. In particular, clutter distributions in three different dimensions are discussed in detail. First a three-term model for the dependence of land clutter on grazing angle is proposed. The model is site-specific and landcover-dependent. Parameters for dominant types of landcover in the Northern Territory region are regressed using AirSAR and MCARM measurements as well as others available in literature. Clutter spatial distribution is also investigated. Aimed at real-time implementation, a simple and fast parameter estimation scheme for the Weibull and K-distributions is given. The estimates are found to be nearly identical to the maximum likelihood estimates. Discussed finally in the report is the clutter temporal distribution (Doppler spectrum) due to motion of moving parts of scatterers. Billingsley's exponential decay model is summarised.

APPROVED FOR PUBLIC RELEASE

Published by

DSTO Systems Sciences Laboratory
PO Box 1500
Edinburgh South Australia 5111

Telephone: (08) 8259 5555
Fax: (08) 8259 6567

AR-013-074
March 2004

Models of Land Clutter vs Grazing Angle, Spatial Distribution and Temporal Distribution – L-Band VV Polarisation Perspective

EXECUTIVE SUMMARY

Radar clutter is defined as unwanted echo. For an AEW&C (airborne early warning and control) radar system operating in a Doppler mode primarily for detecting, tracking and classifying distant aircraft, missiles and possibly other moving targets on the sea and ground, clutter principally comprises return signals from land, the sea, birds, rain, snow, chaff, etc. This report mainly considers land clutter from a L-band VV polarisation perspective.

Because terrain parameters are random, their nature determines land clutter to be random and to vary in many dimensions. Given a radar system (the frequency, polarisation and resolution are thus determined) and a specific type of terrain cover (terrain parameters are also statistically determined), there are still at least three distributions that need to be addressed, namely,

- Distribution against grazing angle;
- Spatial distribution (for a constant grazing angle);
- Temporal distribution (Doppler spectrum caused by motion of moving components of vegetated and water surfaces under wind conditions).

This report focuses on modelling of the above three distributions.

Dominant scattering mechanisms of a surface at different grazing angles are different. In general grazing angles can be divided into three reasonably distinct regions: near grazing incidence, plateau and near vertical incidence. In each of these regions the dependence of surface clutter on grazing angle can be characterised to some extent. A three-term model for the dependence of clutter on grazing angle has been proposed. These three terms model clutter behaviour in the near grazing incidence, plateau and near vertical incidence regions, respectively. The model is site-specific and landcover-dependent, i.e., parameters for different types of landcover are supposed to be different. Based on measurements of the AirSAR and MCARM systems as well as measurements compiled by other researchers, parameters for dominant types of

landcover in the Northern Territory region including eucalypt open woodland/forest, mangrove, shrub/short vegetation, grassland/bare soil and calm river water, have been regressed. Comparisons between the regressed curves and available measurements have shown good agreement.

Also discussed is the clutter spatial distribution. For the same illumination geometry and a statistically homogeneous clutter environment, clutter echo obeys a random process because scatterers are randomly distributed in space. It has been found that the distribution of low resolution clutter data of homogenous landcover is, or very close to, the Rayleigh distribution, as supported by the theory. If each resolution cell contains only one type of landcover, but the area scanned has more than one type of landcover, then the clutter distribution can be considered as a combination of Rayleigh distributions with different means and different weights. The combined distribution may be approximated as the Weibull or K- distribution. Agreeing with others, we have also found that the distribution of sea clutter acquired by a high resolution X-band VV radar at near zero degree grazing angle is approximately the lognormal distribution. A sea surface may be homogenous, but individual cells may not when the resolution is high, leading to the random process not being fully developed. Effects of shadowing and multipath propagation may become dominant at low grazing angle. All these break the criterion of Rayleigh distribution.

The Weibull, K- and lognormal distributions are the most commonly used to approximate the spatial distribution of surface clutter. Depending on data, one may be found to be better than the others for approximating the distribution. The Weibull and K-distributions are very similar and the differences between the two are small for those distributions whose shape parameter is not far from the Rayleigh distribution. The lognormal distribution is usually applied to high resolution and low grazing angle data collected from sea surface or areas containing strong discrete scatterers including buildings and other man-built targets. The lognormal distribution converges the slowest, which is sometimes referred to as having the longest tail.

Fast parameter estimation is an issue given a distribution model and sample data, if the estimation is to be implemented in real-time. Estimates obtained using the maximum likelihood (ML) method are the optimal. Except for the lognormal distribution, the ML estimates for both the Weibull and K- distributions require an iterative algorithm manipulating sample data. The size of sample data sets is usually large in order to obtain reliable statistics, so the iterative algorithm is slow. Aimed at real-time implementation, a fast and simple parameter estimation scheme, named as NB-II (no bias II), is proposed. The NB-II estimation scheme uses the arithmetic mean and the geometric mean to estimate parameters, so the estimated distribution has no bias with respect to the arithmetic mean and the geometric mean of the sample data. The NB-II estimates have been found to be nearly identical to the ML estimates, and can be considered as the asymptote to the ML estimates.

The clutter temporal distribution, or equivalently the Doppler spectrum caused by motion of moving parts of scatterers has also been addressed. The Doppler frequency of L-band land clutter is low and decays rapidly. We do not have proper measured data to investigate. The discussion has been mainly based on available material from the open literature. An exponential decay model and its associated parameters for various landcover, wind condition and radar frequency, proposed by Billingsley (2002), has been summarised in the report. The main points include (1) the Doppler velocity decays exponentially; (2) the shape parameter of the decay function is only dependent on wind conditions and largely independent of radar frequency; (3) the ratio of dc component to ac component of the Doppler spectrum depends on wind conditions, type of landcover and radar frequency but is independent of polarisation.

Author

Yunhan Dong
Electronic Warfare Division

Dr Yunhan Dong received his Bachelor and Master degrees in 1980s in China and his PhD in 1995 at UNSW, Australia, all in electrical engineering. He then worked at UNSW from 1995 to 2000, and Optus Telecommunications Inc from 2000 to 2002. He joined DSTO as a Senior Research Scientist in 2002. His research interests are primarily in radar signal and image processing, and radar backscatter modelling. Dr Dong was a recipient of both the Postdoctal Research Fellowships and Research Fellowships from the Australian Research Council.

Contents

1. Introduction

Radar clutter is defined as unwanted echo. For an AEW&C (airborne early warning and control) radar system operating in a Doppler mode primarily for detecting, tracking and classifying distant aircraft, missiles and possibly other moving targets on the sea and ground, clutter principally comprises return signals from land, the sea, birds, rain, snow, chaff, etc. This report mainly considers land clutter for L-band VV polarised monostatic radar.

Land clutter is a function of many parameters including (Billingsley, 2002):

- Radar parameters, namely, frequency, polarisation and resolution;
- Geometry of illumination, namely, grazing/depression angle; and
- Terrain parameters, namely, landcover and terrain slopes.

Because terrain parameters are random, their nature determines land clutter to be random and to vary in many dimensions. Given a radar system (the frequency, polarisation and resolution are thus determined) and a specific type of terrain cover, there are still at least three distributions we need to address, namely,

- Distribution against grazing angle;
- Spatial distribution (for a constant grazing angle);
- Temporal distribution (Doppler spectrum induced by motion of moving components of vegetated and water surfaces under wind conditions).

Due to the complexity of land surface itself and insufficient mathematical descriptions for it, theoretical models of land clutter in general serve to provide an understanding of the principles and concepts of backscatter under various conditions. Theoretical models are accurate only when environmental conditions match model assumptions, but unfortunately such conditions can only exist in laboratories. Empirical and statistical models on the other hand emphasise measurements and data analysis to avoid seemly endless mathematical modelling. It is believed on the historical evidence that a successful modelling approach would have to be strongly empirical and site specific (Billingsley, 2002).

Based on analysis of L-band VV synthetic aperture radar (SAR) and real aperture radar (RAR) data, this report addresses the above three distributions of land clutter. A statistical model for dependence of clutter on grazing angle, consisting of three terms, corresponding to clutter in the near grazing incidence, plateau and near vertical incidence regions, respectively, is proposed. Parameters of the model may be determined accordingly using measured data. Models of the spatial distribution and temporal distribution of clutter are also discussed in detail.

In addition to the three distributions, many relevant issues of land clutter are also discussed in order to describe its nature.

2. Basics of Clutter

2.1 Definition of Clutter

Because of distributed scatterers, surface clutter is normally described by the radar cross-section (RCS) per unit area of the clutter surface, which is referred to as the backscattering coefficient (σ_0), or the reflectivity, or clutter coefficient, or simply clutter depending on interests, and hence is a dimensionless quantity[1]. For a given transmitter frequency, the power of the return received from the illuminated patch of ground is (Skolnik, 2001),

$$P_r = \frac{P_{avg} G_r G_t \lambda^2 \sigma_0 F^4 A_g}{(4\pi)^3 R^4 L} \tag{1}$$

where P_{avg} - average transmitted power, G_r and G_t - gains of radar receiver and transmitter antennas in the direction, λ - wavelength, A_g - resolvable area of the ground, R - range of the ground patch , F^4 - the pattern propagation factor and L - the total loss including propagation loss and system loss.

For a point target, it is not only difficult but also critical to separate the effect of the propagation factor from the RCS for target identification. In the clutter situation, it is also difficult but may not be necessary to separate the effect of the propagation factor, if we view the distributed scatterers and the Earth surface as a whole. Rigorously speaking, the measured clutter we often refer to is $\sigma_0 F^4$, but not σ_0, because the effect of propagation is automatically included in measurements.

Dominant scattering mechanisms at different incidence angles are different, leading to clutter dependent on incidence/grazing angle, which is detailed in Section 4. The definition of backscattering coefficient implies that its mean value is independent of spatial resolution. However, the individual spatial samples of clutter as opposed to their mean, usually depend strongly on the resolution size (Billingsley, 2002). In a situation where dimensions of discrete scatterers, such as buildings, compared to the radar resolution, are not very small, reducing cell size results in more cell-to-cell variability. Similarly at low grazing angles the effects of shadowing and multipath propagation may dominate, leading to a spread in clutter distributions. Thus the shapes of the broad amplitude distribution of clutter are highly dependent on resolution. Section 5 details clutter spatial distribution. Also according to the definition,

[1] Whilst dimensionless, σ_0 is popularly expressed as m^2/m^2 in the linear scale and dBm^2/m^2 in the dB scale. This report simply expresses it as dB in the dB scale.

clutter should be independent of methods and/or techniques used in measurement. Unfortunately, clutter at near vertical incidence becomes dependent on measuring techniques, which will be addressed in Section 4.

2.2 Propagation Factor

Due to the existence of the Earth which reflects incidence waves, a target at any point within line of sight with a radar antenna above the Earth can receive a direct ray from the transmitter and an indirect ray reflected from the Earth's surface. Figure 1 shows the combination of four possible radar-target paths which normally lead to fluctuations in the measured RCS even though the RCS of the target itself remains constant. Depending on the path length difference, the sum of backscattered field from the four possible paths may be enhanced or reduced. The propagation factor F in general is used to denote the effect of multipath propagation. Assuming the Fresnel reflection coefficient of the Earth surface to be unity, F varies from 0 to 2 (or F^4 varies from 0 to 16).

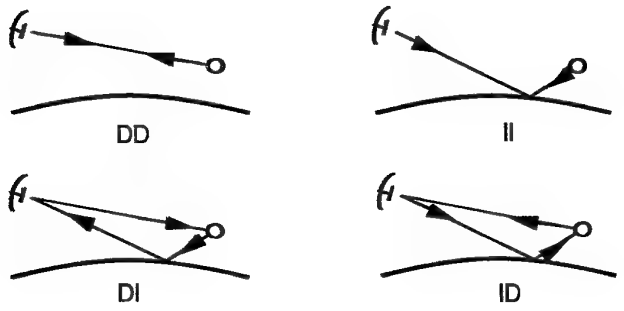

Figure 1: Four possible radar-target paths due to reflections of the Earth. D and I denote direct and indirect reflections (Long, 1992).

In general the effect of multipath propagation may become critical only when a target is close to the Earth surface and the grazing angle is low (Long, 1992). This has to be dealt with carefully. For instance, when the backscattered field is enhanced due to multipath propagation, the measured RCS of a helicopter may be comparable to that of a bomber, or vice versa.

If there is confidence in the propagation factor F^4, the 'true' clutter coefficient σ_0 can be estimated through radar measurements. However, clutter data are often collected without measuring or estimating F^4. Fortunately the attempt to separate the propagation factor in the land clutter situation becomes less critical due to the fact that surface scatterers and the Earth surface itself are always associated together so that they can be considered as a whole. For example, the RCS of a tree without the ground may be significantly different from that of the tree with the ground. However in reality, if there is a tree there must be an associated ground. In the absence of the confident

propagation factor F^4, the clutter coefficient, we refer to, normally does not exclude the propagation factor, and should be explicitly expressed as $\sigma_0 F^4$ as Billingsley (2002) does. No attempt has been made to separate the F^4 factor from the radar clutter data in this report. Therefore the clutter coefficient, we refer to, should be understood as $\sigma_0 F^4$ in general.

2.3 Propagation in the Atmosphere

Microwaves travel in a line of sight fashion in a medium of constant permittivity and permeability (free space is a special case of a medium of constant permittivity and permeability). Densities and constituents of air and other particles such as water vapour and various dusts vary with the height above the Earth, leading to variations in permittivity, so that the so-called refractive index of the atmosphere also varies with the height. As a consequence, rays representing microwave propagation bend. Therefore when an airborne radar looks down to the Earth, its horizon is usually greater than the optical horizon. A standard way to 'stretch' bending rays straight to compensate the effect of the gradient of refractive index with respect to height is to replace the actual Earth's radius r by an effective Earth's radius r_e. The use of the average value of the gradient of refractive index with respect to height leads to a value of $r_e = 4/3r$ (Kerr, 1951, Long, 1992, 2001), which is commonly called the four-thirds Earth model.

It should be pointed out that the four-thirds Earth model is only a general approximation to the effects of refraction in atmosphere. It has been found that 95+% propagation deviates more or less from this approximation especially at low to very low grazing angles on water surfaces. The typical value of the gradient of refractive index with respect to height is $-3.9\times10^{-8}m^{-1}$. If this value becomes less than $-16\times10^{-8}m^{-1}$, the radius of the curvature of transmitted rays will be less than or equal to the radius of curvature of the Earth. Such effect is also known as ducting, trapping or waveguide propagation (Long, 1992).

2.4 Resolution Cell

The resolution cell (illuminated patch) for a radar looking at the surface of the Earth is depicted in Figure 2 (a) where the range resolution is determined by the pulse length. The area of the cell is,

$$A_g = \left(\frac{c\tau}{2}\sec\beta\right)(\theta_a R\cos\alpha) \approx \frac{c\tau}{2}\theta_a R \qquad (2)$$

where α and β are the depression angle and grazing angle, respectively and $\cos\alpha \approx \cos\beta$. θ_a is the azimuth beamwidth angle, τ the pulse length (often compressed), c the speed of light and R the range.

In this pulse length limited case, the resolution cell is proportional to the range, so the received clutter power is inversely proportional to R^3.

For near vertical incidence, pulse length usually does not effect the resolution cell. It then becomes the so-called beamwidth limited case, and the resolution cell is determined by the beamwidths of azimuth and elevation angles. For an antenna lobe of approximately elliptical shape with 3dB azimuth angle θ_a and elevation angle θ_e as shown in Figure 2 (b), the illuminated area may be approximated by an ellipse with an area of (Long, 2001),

$$A_g = \pi(R\theta_a/2)(R\theta_e \csc\alpha/2) = \pi R^2\theta_a\theta_e \csc\alpha/4 \qquad (3)$$

In this beamwidth limited case, the resolution cell is proportional to R^2, so the received clutter power is inversely proportional to R^2.

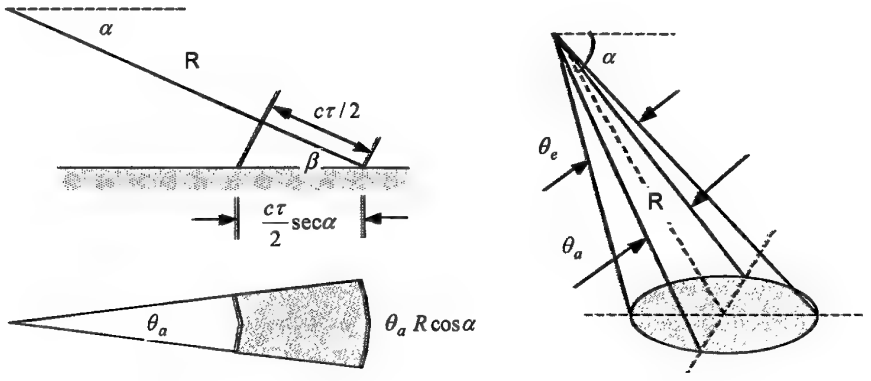

Figure 2: Resolution cell for radar looking at the surface of the Earth: (a) pulse limited case and (b) beamwidth limited case.

3. General Behaviour of Clutter

3.1 Dependence of Clutter on Surface Roughness

Surface roughness is generally described by its surface root mean square (rms) height and the correlation length (Ulaby et al, 1982). A surface with a shorter correlation length appears rougher than a surface with a longer correlation length, even though the rms heights of both surfaces are the same. Given a surface in the $x-y$ plane whose height at a point (x,y) is $z(x,y)$, its rms height s is,

$$s = \left[E\{[z(x,y) - \overline{z(x,y)}]^2\}\right]^{1/2} = \left[\overline{z^2} - \overline{z}^2\right]^{1/2} \tag{4}$$

The normalised autocorrelation coefficient for a one-dimensional surface profile $z(x)$ is defined as

$$\rho(\Delta x) = \frac{\int_{-\infty}^{\infty} z(x)z(x+\Delta x)dx}{\int_{-\infty}^{\infty} z^2(x)dx} \tag{5}$$

The correlation length is usually defined as the displacement Δx for which $\rho(\Delta x)$ is equal to $1/e$.

$$\rho(l) = 1/e \tag{6}$$

The correlation length provides a reference for estimating the statistical independence of two points on the surface. If two points are separated by a distance greater than l, their heights may be considered to be statistically independent (Ulaby et al, 1982). On a perfect smooth surface, the height of every point is correlated to the height of every other point with correlation coefficient of unity. Hence in this case $l = \infty$.

Conceptually the relationship between surface roughness and surface scattering can be illustrated in Figure 3. A perfectly smooth surface acts like a mirror and refects all incident waves obeying the Fresnel reflection law. For a slightly rough surface, the radiation pattern consists of two components: a reflected component in the specular direction and a scattered component in all directions. The amplitude of the reflected and scattered components varies depending on the surface roughness. As a surface becomes rougher and rougher, the reflected component vanishes and the scattered field is equally radiated in all directions; in this situation the surface is also called a Lambertian surface (Lambert's law[2]).

Figure 3: Dependence of surface scattering on the surface roughness (Ulaby et al, 1982).

[2] Lambert's law was named after the paper published in *Photometrica*, 1760, by Lambert, J H.

A surface can be either rough or smooth relative to wavelength. A Lambertian surface to optical wave may appear smooth to microwave. In general the Rayleigh criterion for a smooth surface is (Ulaby et al, 1982)[3],

$$s < \frac{\lambda}{8\cos\theta} \tag{7}$$

where θ is the incidence angle. A more stringent criterion (Fraunhofer criterion) for a smooth surface is

$$s < \frac{\lambda}{32\cos\theta} \tag{8}$$

In practice, asphalt surfaces including runways, freeways and highways may be considered smooth for all radar frequencies. It is worth noting that the relative roughness of a surface depends on not only the wavelength but also the incidence angle. A surface always appears smoother at larger incidence angles (smaller grazing angles).

The clutter coefficient of a rough surface is governed by roughness (relative to the wavelength) and dielectric properties of the surface, as well as incidence angle. Figure 4 shows angular patterns of surface clutter for five bare-soil fields with different scales of roughness. The moisture contents of all five fields are similar, so the dielectric constants of all fields can be considered approximately the same. The differences in clutter are therefore mainly due to the surface roughness. For the same soil field, the surface is smoother relative to L-band than to C-band, so that more incident energy is specularly reflected is the former case. As a consequence, the dependence of clutter on incidence angle at lower frequencies is more distinct for less rough surfaces. According to the figure, the soil field with an rms height of 4.1cm (in the order of the wavelength) at C-band acts almost like a Lambertian surface and its clutter shows little dependence on incidence angle.

[3] The Rayleigh criterion for a smooth surface was first published by Lord Rayleigh in *Phil Mag.*, 8, 403, 1879 (reprinted in *Scientific Papers*, Cambridge Univ Press, 1, 432-435, 1899).

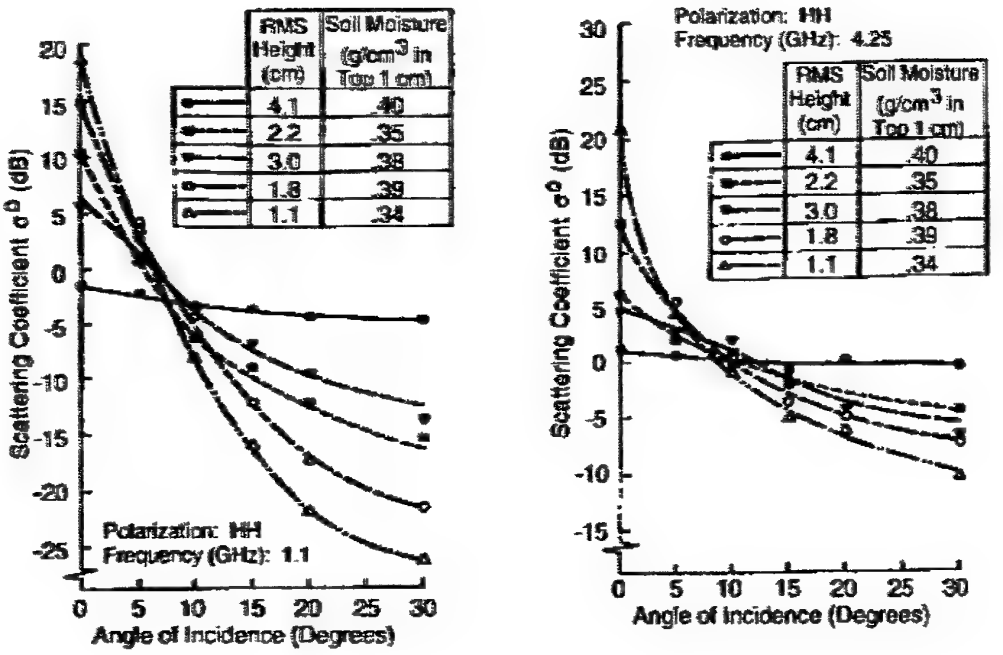

Figure 4: Angular patterns of clutter for bare soil with different roughened surfaces at L-band and C-band. (Ulaby et al, 1982).

3.2 Dependence of Clutter on Surface Moisture

The dielectric constant of soil is dominated by its water content. Consequently even if the roughness of a surface remains unchanged, its σ_0 may exhibit a dynamic range of about 10dB between very dry and very wet soil conditions (Ulaby and Dobson, 1989). To examine the dynamic range of σ_0 due to changes in the surface moisture, we assume all radar and soil parameters unchanged except the moisture. Small perturbation techniques have been successfully used to model backscatter from slightly rough surfaces such as ground and sea surfaces (Elachi, 1987, Rice, 1951, and Valenzuela, 1967). The model itself is mathematically complicated, but for our purpose its implicit form can be written as,

$$\sigma_0 = |\alpha_{pp}|^2 f(s,l,\theta,\lambda) \qquad (9)$$

where $f(\cdot)$ is a function of radar and surface roughness parameters, and independent of the dielectric constant of the surface. The Bragg[4] scattering coefficient α_{pp} is a function of dielectric constant as (Elachi, 1987),

[4] Bragg equation and angle diffraction was named after the paper published in *Proc. Cambridge Phil. Soc.*, 1912 by Bragg, W L.

$$\alpha_{vv} = (\varepsilon_r - 1)\frac{\varepsilon_r\left(\sin^2\theta + 1\right) - \sin^2\theta}{\left(\varepsilon_r \cos\theta + \sqrt{\varepsilon_r - \sin^2\theta}\right)^2} \tag{10}$$

$$\alpha_{hh} = \frac{\varepsilon_r - 1}{\left(\cos\theta + \sqrt{\varepsilon_r - \sin^2\theta}\right)^2} \tag{11}$$

where ε_r is the relative dielectric constant of the surface.

The dielectric constant can be as low as $3 - i0$ and as high as $79 - i1.5$ for very dry and freshwater saturated sandy loam, respectively, at L-band (Boyarskii et al, 2002). Given an incidence angle of 45° we calculate the difference between the backscattering coefficients of the wet and dry soil surface to be 8.1dB for VV polarisation and 6.9dB for HH polarisation.

The small perturbation model only applies to a slightly rough surface. For a statistically rough surface, the backscatter model may be written as (Ruck et al, 1970),

$$\sigma_0 = \left|R_{pp}\right|^2 g(s, l, \theta, \lambda) \tag{12}$$

where R_{pp} is the Fresnel reflection coefficient and its expression is (Ruck et al, 1970, Ulaby et al, 1982)[5],

$$R_{vv} = \frac{\varepsilon_r \cos\theta - \sqrt{\varepsilon_r - \sin^2\theta}}{\varepsilon_r \cos\theta + \sqrt{\varepsilon_r - \sin^2\theta}} \tag{14}$$

$$R_{hh} = \frac{\cos\theta - \sqrt{\varepsilon_r - \sin^2\theta}}{\cos\theta + \sqrt{\varepsilon_r - \sin^2\theta}} \tag{15}$$

Again for very dry and freshwater saturated sandy loam with dielectric constants of $3 - i0$ and $79 - i1.5$, respectively, at L-band, and given an incidence angle of 45°, we calculate the difference between the backscattering coefficients of the wet and dry soil surface to be 13.9dB for VV polarisation and 7.0dB for HH polarisation.

Figure 5 shows the radar response to changes in soil moisture of a slightly rough surface and a rough surface at an incidence angle of 20° at L-band with HH polarisation. It can be seen that the slopes of two regressed linear lines are

[5] Fresnel's law was named after the paper published in *Mem. de l'Acad*, 1832 by Fresnel, A.

approximately the same, confirming that the change in the backscattering coefficient with respect to moisture is independent of surface roughness.

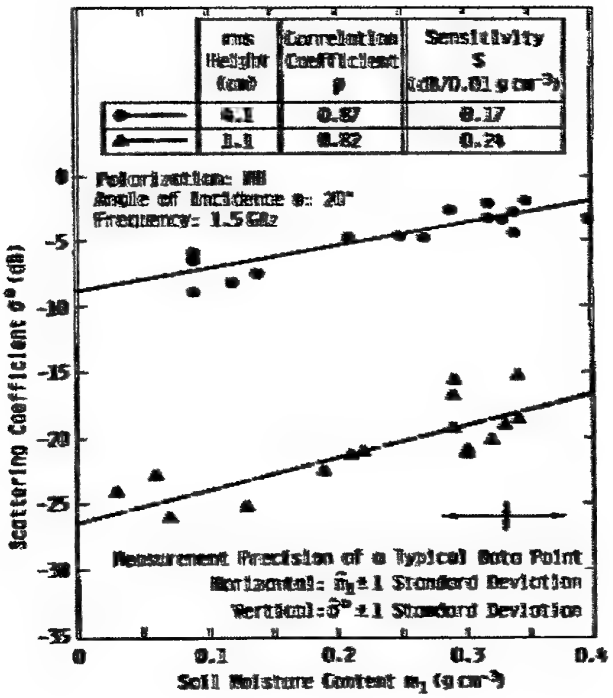

Figure 5: Clutter variation with the soil moisture content measured at an incidence angle of 20° at L-band with HH polarisation (Ulaby and Dobson, 1989).

Water content controls not only dielectric properties of soil but also growth of vegetation. In regions with monsoonal climate such as the Darwin region, herbaceous plants periodically die in the dry season and flourish in the wet season. Woody plants do not die in the dry season, but usually have much less leafing material in order to survive. Figure 6 (a) shows the growth in understorey vegetation in January, the height of the wet season in Kakadu National Park (13.0°N, 132.5°E). The same scene in October, Figure 6 (b), near the end of the dry season, has virtually no herbaceous plant material. The corresponding clutter might be different, not only due to more or less of the understorey vegetation and leafy biomass of trees, but also due to the significant difference in the dielectric constants of the ground surface between dry and wet seasons. The seasonal changes of deciduous trees and cultivated land will also result in clutter dynamics.

(a) (b)

Figure 6: The appearance and disappearance of understorey vegetation in wet and dry seasons, respectively. Photos were respectively taken in January and October in Kakadu National Park (AUSLIG, 1990)

The dynamic change of clutter due to moisture content of a soil surface can be demonstrated by SAR images collected in different seasons. Figure 7 shows a sequence of RADARSAT (C band, HH polarisation) SAR images of the South Alligator River (12.3°N, 132.4°E), the Northern Territory (NT), acquired in February, May and September, respectively, in 1998 (Horn et al 2001). The September (end of the dry season) image, Figure 7 (c), clearly depicts the South Alligator River and its adjacent floodplain whose grassland cover retained only isolated patches of trees or woodland. The February image (middle of the wet season), Figure 7 (a), shows the widespread nature of the wet conditions. Due to the extensive grass cover of the floodplain initiated by rain, the boundary between the saturated floodplain and the saturated woodland became difficult to detect as shown in Figure 7 (b). Some bright patches (possibly shrubs or small trees) in the floodplain area shown in the wet season image disappeared in the dry season image indicating that these areas were possibly flooded when the wet image was taken, so that there might be a strong component of double bounce return in the wet image for these areas.

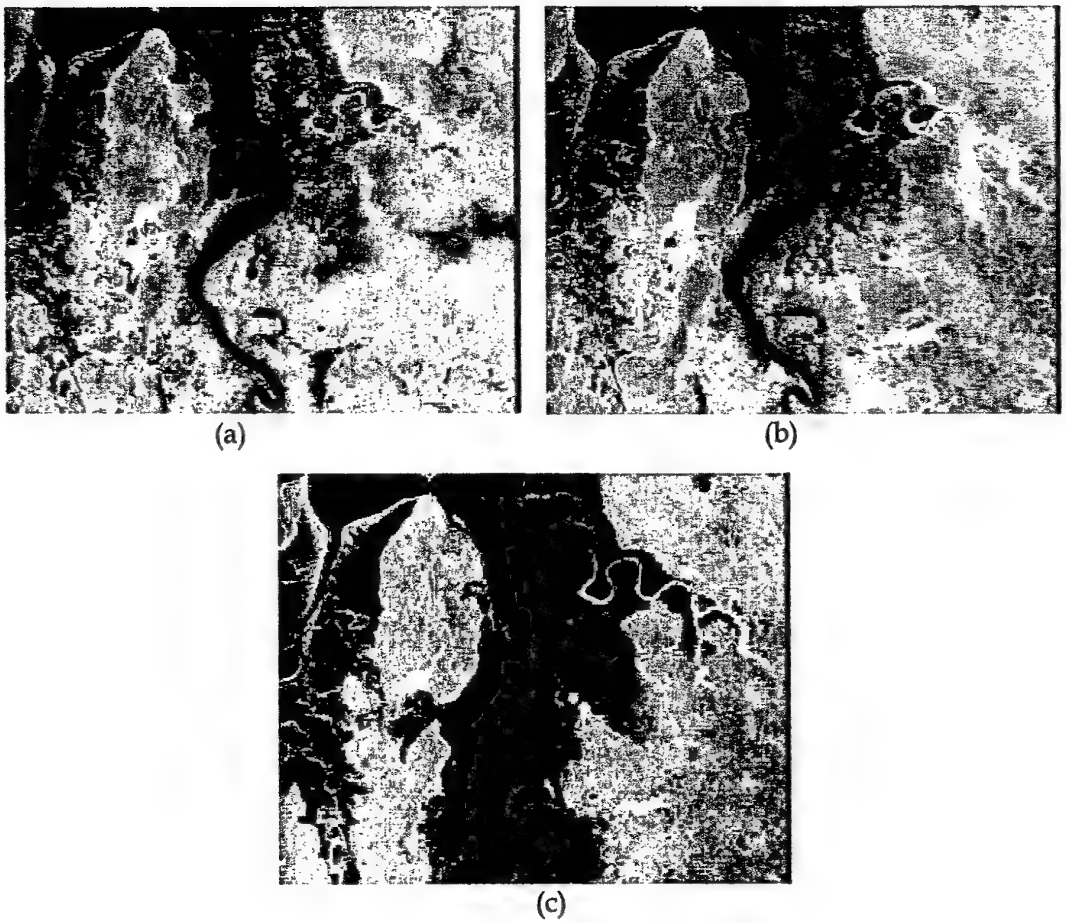

Figure 7: RADARSAT C band HH multi-temporal imagery of South Alligator River, the Northern Territory, acquired in (a) February, middle of the wet season, (b) May, end of the wet season and (c) September, end of the dry season, 1998, respectively (Horn et al, 2001).

3.3 Dependence of Clutter on Polarisation

Clutter is usually polarisation dependent. The ratio of σ_{0hh} to σ_{0vv} is referred to as polarisation index (PI). Observation indicates that σ_{0vv} is usually higher than σ_{0hh} for sea and bare soil surfaces at low grazing angles. This might be explained by the small perturbation model. According to (9), the PI of a slightly rough surface is,

$$PI = \left|\alpha_{hh} / \alpha_{vv}\right|^2 \tag{16}$$

For seawater having $\varepsilon_r = 79 - i59$ and bare soil having $\varepsilon_r = 15 - i3$ we calculate $PI = -8.4dB$ for seawater and $PI = -6.7dB$ for bare soil at $\theta = 45^0$. Figure 8 shows L-band HH and VV clutter of seawater acquired by the NASA/JPL AirSAR system in 2000. The Bragg scattering usually dominates at low grazing angle, results in σ_{0vv} to be higher than σ_{0hh}.

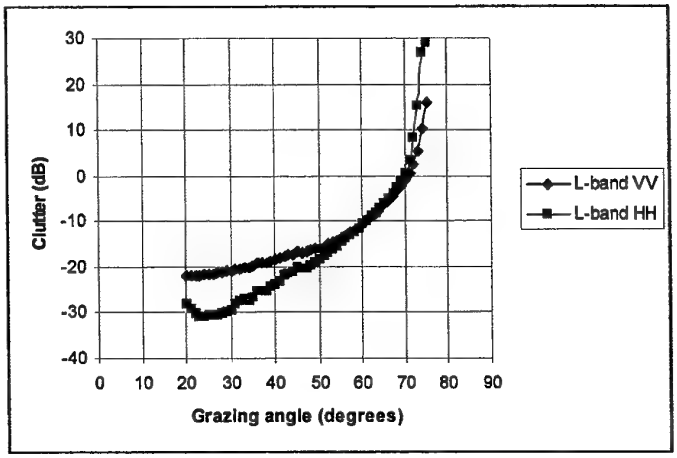

Figure 8: HH and VV Clutter of seawater (the Darwin scene) at L-band acquired by the JPL AirSAR system[6].

However, non-Bragg scattering mechanisms will become dominant when the grazing angle is at the vicinity of the Brewster angle (about 6° for seawater) or even lower (Trizna, 1997, Lee, et al, 1994). In this grazing angle region, effects of the Brewster angle damping, shadowing, and multipath propagation dominate backscatter. Because of Brewster angle effects, the forward scatter path from the water surface is severely damped for the vertical polarised waves, producing much weaker multipath propagation effects for the VV backscatter than that for the HH backscatter. Since the multipath propagation effects can be constructive and destructive, the oscillation of the HH backscatter is generally greater (Long, 2001, Trizna, 1997). Moreover, the PI value will be generally greater than 1. For instance, a 6dB or greater PI index has been observed for the sea surface with light wind conditions at a grazing angle of 2°, using a X-band offshore marine radar (Trizna, 1997).

For a statistically rough surface, if the backscatter model (12) applies, the PI becomes,

[6] Values when the grazing angle is greater than 70° seem questionable. The values are too high and the difference between the two is too large. This is possibly due to the calibration, as the calibration of a beamwidth-limited limited case (near vertical incidence) differs to the calibration of a pulse-limited case (low to medium grazing incidence). See Section 2.4.

$$PI = \left| R_{hh} / R_{vv} \right|^2 \tag{17}$$

In this situation, the value of PI is normally grater than 1 indicating σ_{0hh} higher than σ_{0vv}. Again we calculate $PI = 1.2dB$ and $PI = 3.2dB$, respectively, for seawater having $\varepsilon_r = 79 - i59$ and bare soil having $\varepsilon_r = 15 - i3$, at an incidence angle of 45°. However when the incidence angle approaches vertical, there is no discrimination between the two polarisations for natural surfaces; σ_{0hh} and σ_{0vv} become identical regardless of surface roughness, moisture content etc.

From the above descriptions, the dynamic range of HH for grazing angle ranging from zero to 90 degrees is usually greater than that of VV. This is one of the reasons why HH polarised radar is commonly used in remote sensing for surface mapping to increase sensitivity.

For a vegetated surface such as a forested area, if the foliage layer is not very dense and the wavelength is long (e.g., L-band and longer wavelengths), the trunk-ground double bounce (Richards et al, 1987) might dominate as shown in Figure 9. Since the attenuation of the foliage layer, and diffuse scattering due to the surface roughness of both the trunck and ground surfaces can be considered to have a similar effect on both polarisations, the PI of trunk-ground double bounce is (Dong et al, 1998),

$$PI = \left| \left[R_{hh2}(\pi/2 - \theta) R_{hh1}(\theta) \right] / \left[R_{vv2}(\pi/2 - \theta) R_{vv1}(\theta) \right] \right|^2 \tag{18}$$

where R_{pp1} and R_{pp2} denote the Fresnel reflection coefficients of the ground surface and the trunk surface, respectively.

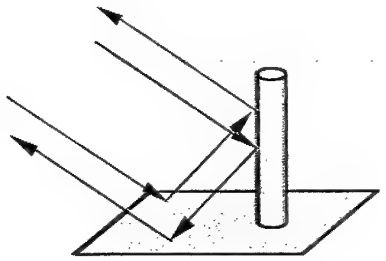

Figure 9: Trunk-ground double bounce scattering.

Given dielectric constants of the trunk and ground surface to be $30 - i6$ (Karam et al, 1992) and $15 - i3$ (Ulaby et al, 1982), respectively, the PI for the trunk-ground double bounce scattering mechanism as a function of incidence angle is shown in Figure 10. It can be seen, the PI value is always greater than 0dB as long as the incidence angle is not equal to 0 or 90 degrees. The two humps shown in the figure are due to the

Brewster angle damping effect of the trunk and ground surfaces, respectively. The PI value is about 5-8dB for the incidence angle in the range of 25-60°.

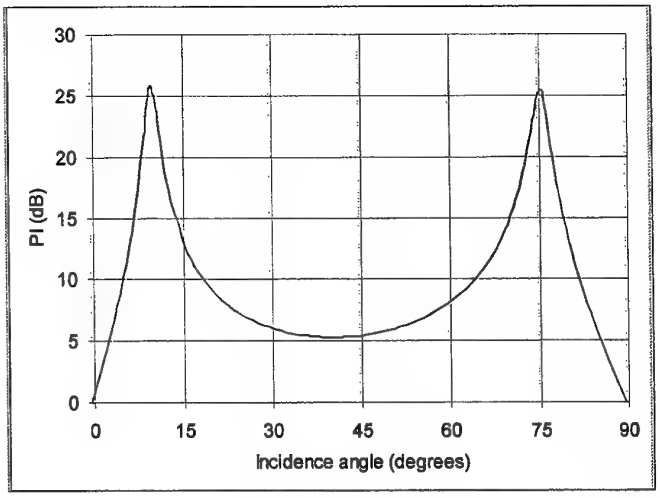

Figure 10: The polarisation index for the trunk-ground double bounce mechanism as a function of incidence angle. The two humps are due to the Brewster angle damping effect of the trunk and ground surfaces, respectively.

Backscatter of forested land often consists of several scattering mechanisms whose PI values differ. For example, the PI value of surface scattering varies from a minus few dB to a plus few dB depending on the scale of the roughness; the PI value is usually 0dB for volume scattering from the foliage layer, if the dimensions of leaves are much smaller than the wavelength and their orientation is random; while the PI value for the trunk-ground double bounce and branch-ground double bounce is a plus few dB. As a consequence the PI value of forested land varies depending on the dominant mechanism(s). Observation indicates that at L-band the PI value of forests tends to be a plus few dB. Figure 11 shows L-band HH and VV clutter of eucalyptus open woodland acquired by the NASA/JPL AirSAR system in which σ_{0hh} is consistently a few dB higher than σ_{0vv} in the plateau region. The PI value for the grazing angle in the plateau region seems to remain approximately constant or slightly increase with respect to the biomass (correlated to density and height of forest stands) of forests in a merely noticeable rate as shown in Figure 12 where the measurements were taken by Dobson and his colleagues (Dobson et al, 1992).

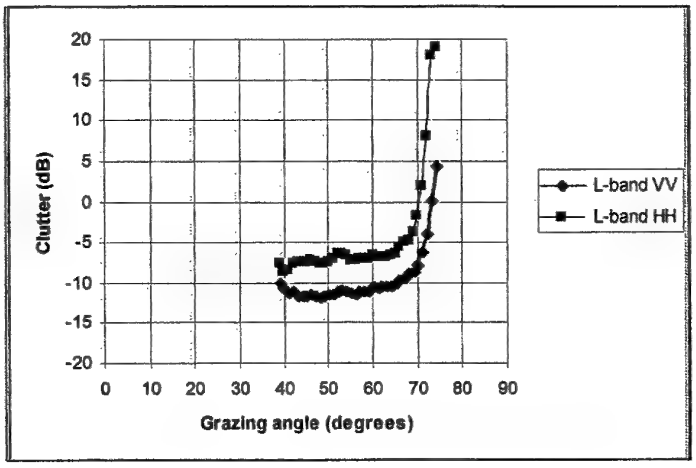

Figure 11: L-band HH and VV clutter of Eucalyptus open woodland in the Darwin area acquired by the JPL AirSAR system[7].

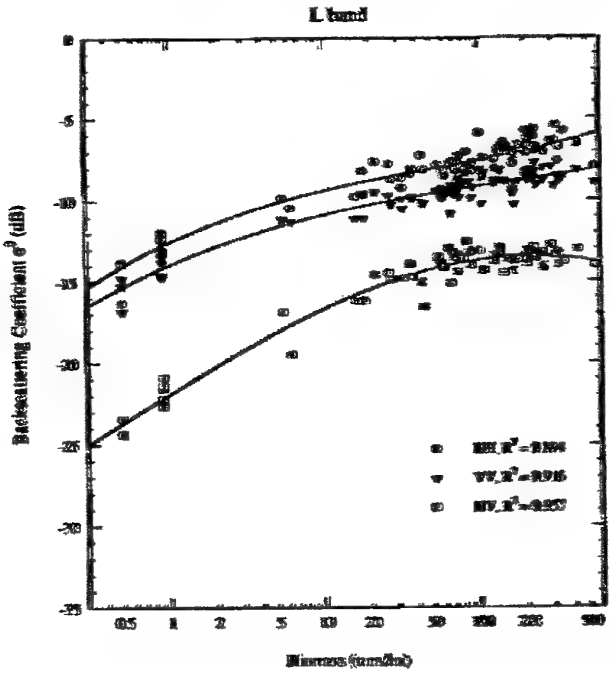

Figure 12: L-band HH, VV and HV clutter variation with the biomass of forests (Dobson et al, 1992).

[7] For the same reason as in Footnote 6, values at high grazing angles seem questionable.

4. Dependence of Surface Clutter on Grazing Angle

4.1 Three Grazing Angle Regions

Figure 13 shows the geometry of an airborne radar looking down on the Earth surface where the effective radius of the Earth r_e has been used to compensate the bending effect of electromagnetic rays due to the gradient of refractive index with respect to the height. Three angles, α, θ and β denote depression angle, incidence angle and grazing angle, respectively, and α and θ are of mutually complementary angles. Due to the curvature of the Earth surface, the grazing angle is generally less than the depression angle especially when the depression angle is small and the range long. It is not difficult to determine their relationships. However in circumstances of the existence of local slopes in hilly areas, the grazing angle is related to not only the depression angle and the range, but also the local slopes. In this situation TED (terrain elevation data) may be used to determine the actual grazing angle.

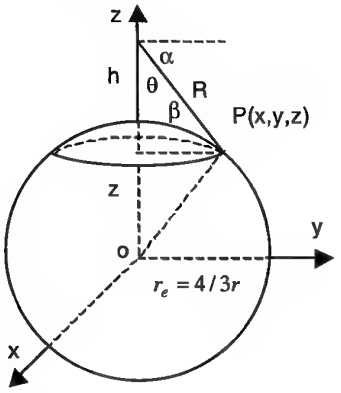

Figure 13: Geometry of airborne radar looking down to the Earth surface.

Dominant scattering mechanisms of a surface at different grazing angles are different. In general, grazing angles can be divided into three reasonably distinct regions: near grazing incidence, plateau and near vertical incidence (Long, 2001). In each of these regions, the dependence of surface clutter on grazing angle can be characterised to some extent. For instance, for a rough surface, shadowing and multipath interference may be the dominant scattering mechanisms at the near grazing incidence region, rough surface scattering at the plateau region and facet scattering at the near vertical incidence region as shown in Figure 14. The boundaries of these three regions change with wavelength, polarisation and surface condition.

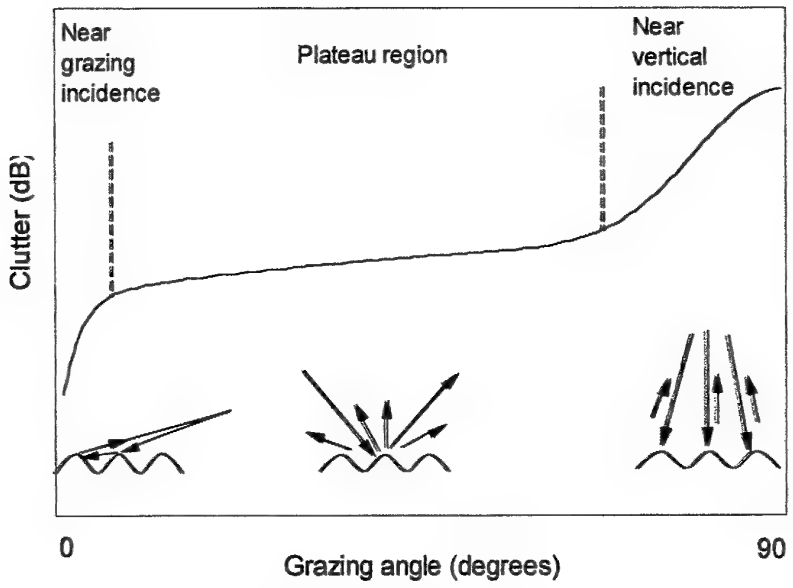

Figure 14: Three grazing angle regions and the corresponding dominant scattering mechanisms for a rough surface.

4.1.1 Near Grazing Incidence Region

Surface clutter at the near grazing incidence region is most difficult to measure and compare. Because of shadowing, multipath interferences and fluctuations of refractive index of the atmosphere, a slight change in measuring conditions might lead to significant changes in measured results. Another factor is that the clutter value at this region is generally very low, close to the noise level of the system. Therefore if a system does not have good linearity at the low signal level, measurements will become questionable.

According to the radar equation (1), the received power of a point target is proportional to R^{-4}. The clutter strength is however proportional to R^{-3} because the illuminated patch is proportional to R as shown in (2). At low grazing angles, it has been found that the drop of clutter strength is much faster and can be proportional to R^{-7} (Katzin, 1957) as shown in Figure 15. For comparison Figure 16 shows received power of a ship (point target) varies with R^{-4} and R^{-8} in near and far ranges, respectively (Long, 2001). The received power versus range of MCARM data (see Appendix A for details) is shown in Figure 17. If we draw R^{-3} and R^{-7} curves over the received power, it seems that part of the curves agree with the drop tendency of the received power as shown Figure 17.

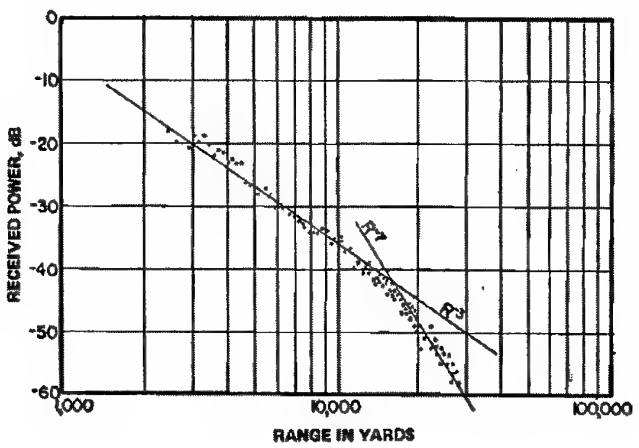

Figure 15: Received sea clutter power versus range. Radar height = 1000ft and wavelength = 3.2cm (Katzin, 1957). The classical 4/3 Earth horizon range is 78,740 yards, far beyond the recorded range. The grazing angle at the range of 15000 yards (the intersection of the R^{-3} and R^{-7} lines) is 1.23°.

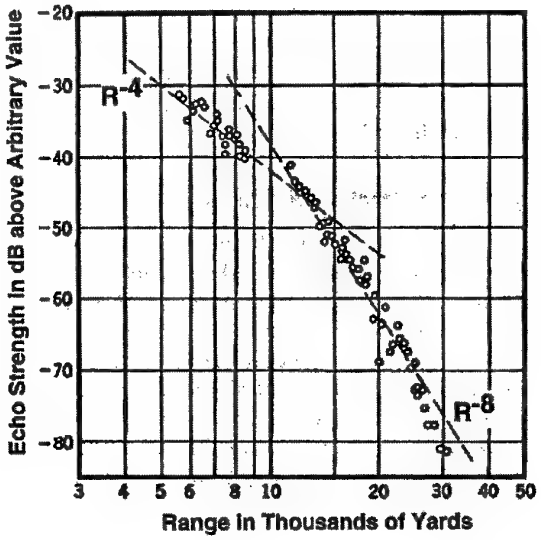

Figure 16: Ship echo as a function of range. Radar height is 125ft and wavelength 30cm. The straight lines correspond to variation of echo strength with R^{-4} and R^{-8}, respectively (Long, 2001). The classical 4/3 Earth horizon range is 27,839 yards. The grazing angle at the range of 12000 yards (the intersection of the R^{-4} and R^{-8} lines) is 0.16°.

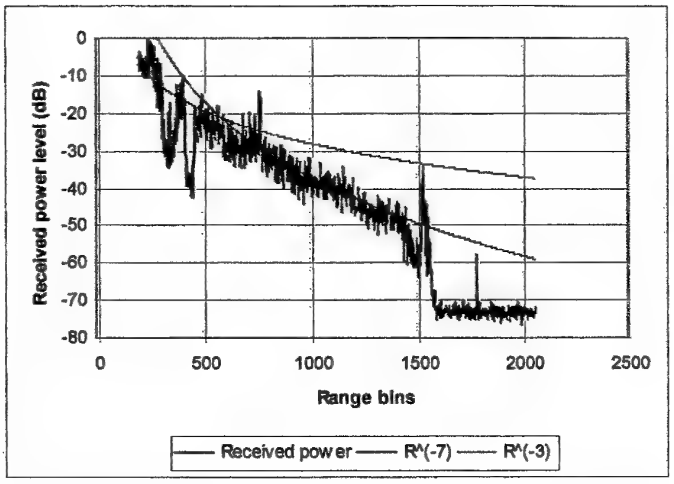

Figure 17: Received power as a function of range (Low PRF MCARM data).

The grazing angles corresponding to R^{-3} and R^{-7} ranges for sea clutter and R^{-4} and R^{-8} ranges for the point target can be estimated by assuming rectilinear propagation with the classical 4/3 Earth model. The results are summarised in Table 1 which includes estimates made for the low PRF MCARM data (Figure 17). It can be seen that the grazing angles of MCARM data is closer to that of Katzin's data (1957); both data were collected from airborne radars. However the corresponding grazing angles for the surface radar (Long, 2001) seem to be significantly smaller than the grazing angles of airborne radars. This might be due to the significant height as well as range differences between surface radars and airborne radars.

Table 1: Grazing angles corresponding to power proportional to R^{-3} and R^{-7} (R^{-4} and R^{-8} for point targets) ranges

Source	Radar and height	Power $\propto R^{-3}$ range and the corresponding grazing angle	Power $\propto R^{-7}$ range and the corresponding grazing angle
Long (2001)	L-band 125 ft (surface)	6000-12000 yd 0.38-0.16°	12000-25000 yd 0.16-0.02°
Katzin (1957)	C-band 1000 ft (airborne)	3000-15000yd 6.37 - 1.23°	15000-30000yd 1.23- 0.54°
This report	L-band 3592 m (airborne)	Range bins 300-500 5.6 - 3.2°	Range bins 700-1400 2.2 - 0.7°

It can be seen in Figure 17 that the intersection area of the R^{-3} and R^{-7} curves does not agree with the clutter echo very well. The dependence of clutter on grazing angle for the MCARM data with the grazing angle plotted in the log scale is shown in Figure 18,

in which both the low PRF and the medium PRF data are shown. Ignoring some spikes in the figure as they are possibly point targets, we can see that there are mainly two levels of clutter as indicated by two dotted lines. In fact they are clutter of farmland and clutter of bay water, respectively (refer to Appendix A for details). As shown in the figure the clutter of bay water drops down to the noise level before the grazing angle reaches to zero degrees, which may be due to ducting, or limitation of dynamic range of the A/D conversion (14-bit conversion was used in the MCARM data). Because the drop of the clutter level (in dB) is approximately linear when the grazing angle is plotted in the log scale, we can conclude that the clutter (in dB) in the near grazing incidence region approximately drops exponentially with the grazing angle.

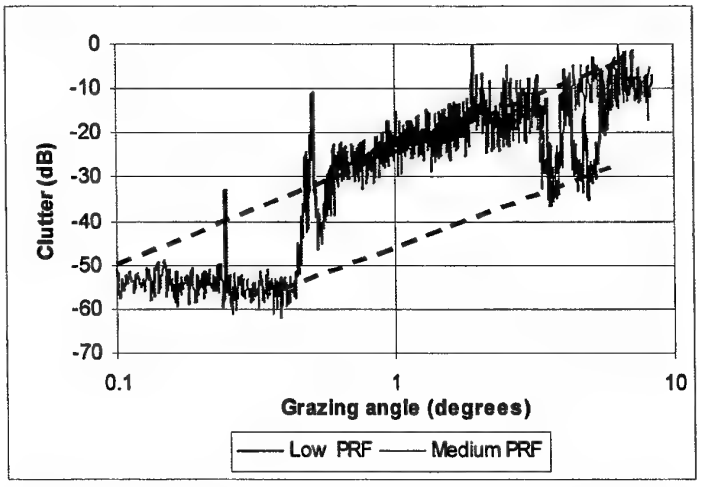

Figure 18: Clutter echo (in dB) drops exponentially with grazing angle in the low grazing incidence region.

4.1.2 Near Vertical Incidence Region

Surface clutter at the near vertical incidence region is also difficult to compare, because the measurement is, to some extent, system dependent, and the antenna pattern plays a significant role in the measurement (Long, 2001). As shown in Appendix B, the clutter coefficient of a flat conducting surface of infinite extent at vertical incidence is dependent on the antenna gain, or equivalently on the beamwidth. A calm water surface may approximate a flat conducting surface condition at microwave frequencies, if the illuminated area is small and the curvature of the Earth can be ignored. When the curvature of the Earth cannot be ignored, the reflected wave spreads, and it can be expected that the backscattering coefficient will decrease, but its dependence on the antenna gain still exists. This illustrates the dependence of surface clutter coefficient at normal incidence on the techniques and methods used in measurement (in contrast to the definition of the surface clutter coefficient, which is supposed to be independent of radar parameters). It has been reported that clutter coefficient of calm seawater at normal incidence varies from +10 to 26dB (Nathanson et al, 1999). It is also worth

noting that at normal incidence, the discrimination of H and V polarisations normally vanishes, unless there are man-made features on the surface, such as power lines parallel to one of the polarisation directions.

4.2 Three-Term Model

A few land clutter models are available in the literature (e.g, Morchin 1990). The scattering at very low and very high grazing angles are extremely complex, and often difficult to model precisely and accurately. We intend to construct a general statistical model as an aid in developing radar design concepts and verifying various radar specifications operating in different environment. After a careful study of characteristics of the dependence of clutter on grazing angle in three different regions, we propose a three-term model as,

$$\sigma_0(\beta) = -c_1 \exp(-k_1\beta) + k_2\beta + c_3 \sin^{\eta}(k_3\beta) + c_0 \qquad 0 \le \beta \le \pi/2 \tag{18}$$

where clutter σ_0 is in dB and grazing angle β in radians. Regression parameters include c_i $i = 0,1,3$, and k_i, $i = 1,2,3$, and η, whose meanings and values will become clear shortly.

For simplicity, we use the word 'curve' to represent surface clutter as a function of grazing angle. The first three terms in (18) represent the shape of the curve at the near grazing incidence, plateau, and near vertical incidence regions, respectively. The fourth term is a constant to adjust the curve's relative position.

At the near grazing incidence the curve is modelled as an exponential function, which is supported by the study of MCARM data as described in Section 4.1.1. Parameter c_1 determines the total variation of clutter in the near grazing incidence region. Parameter k_1 determines the region of near grazing incidence. For instance, if the total variation in the near grazing incidence region is 10dB, let $c_1 = 10$. Also if the variation is 1dB at $\beta = 5^o$, that is, $-10\exp(-k_1 5\pi/180) = -1$, so $k_1 = 26.4$.

The second term represents the curve in the plateau region linearly increasing with a slope of k_2.

The third term represents the curve in the near vertical incidence region. If $k_3 = 1$, parameter c_3 is the extra increment amount at $\beta = \pi/2$ adding to the linear increment of term 2. If $k_3 < 1$, the increment amount reduces to $c_3 \sin^{\eta}(k_3\pi/2)$. The selection of k_3 enables the selection of different parts of the sinusoidal function to represent the behaviour of clutter in the near vertical incidence region. In general, $0.8 \le k_3 \le 1$. The selection of η determines the region of the near vertical incidence, and the higher the value the narrower the region.

The last term c_0 determines the relative position of the curve. In the plateau region, for instance at $\beta = 45^0$, the contribution of both term 1 and term 3 is 0dB, and the contribution of term 2 is $k_2\pi/4$ dB. If the clutter value at $\beta = 45^0$ is $\sigma_0(\pi/4)$, then $c_0 = \sigma_0(\pi/4) - k_2\pi/4$.

Figure 19 shows an example of surface clutter as a function of grazing angle, modelled as a sum of three terms. The values of all parameters used are also given in the figure.

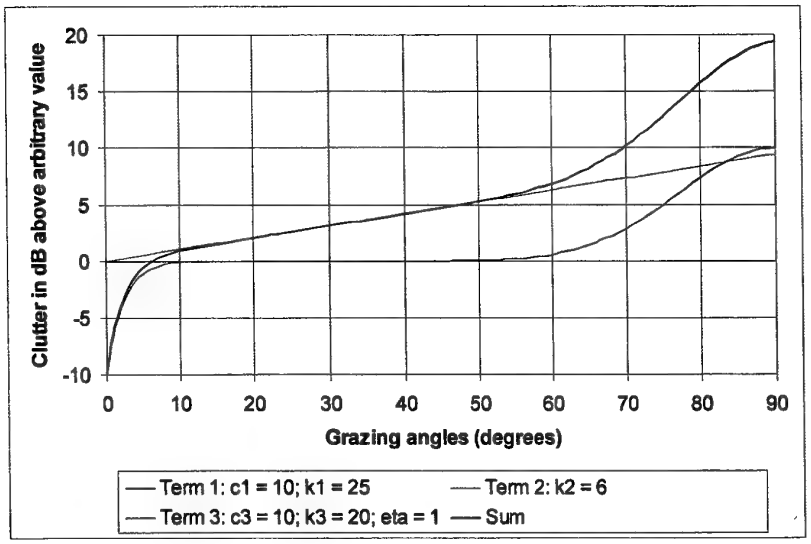

Figure 19: The dependence of surface clutter on grazing angle is modelled as a sum of three terms representing clutter in the near grazing incidence region, plateau region and near vertical incidence, respectively.

A more realistic example is shown in Figure 20. In this example, the measurement is the L-band VV clutter of short vegetation compiled by Ulaby and Dobson (1989). The available data is for grazing angle from 10 to 90 degrees with an interval of 5 degrees. The regressed values for the parameters are, $c_1 = 50$, $k_1 = 45$, $k_2 = 6$, $c_3 = 20$, $\eta = 15$, $k_3 = 0.9$ and $c_4 = -24.4$. It demonstrates that the curve of the 3-term model, when parameters are correctly chosen, can precisely represent the measurement of the clutter.

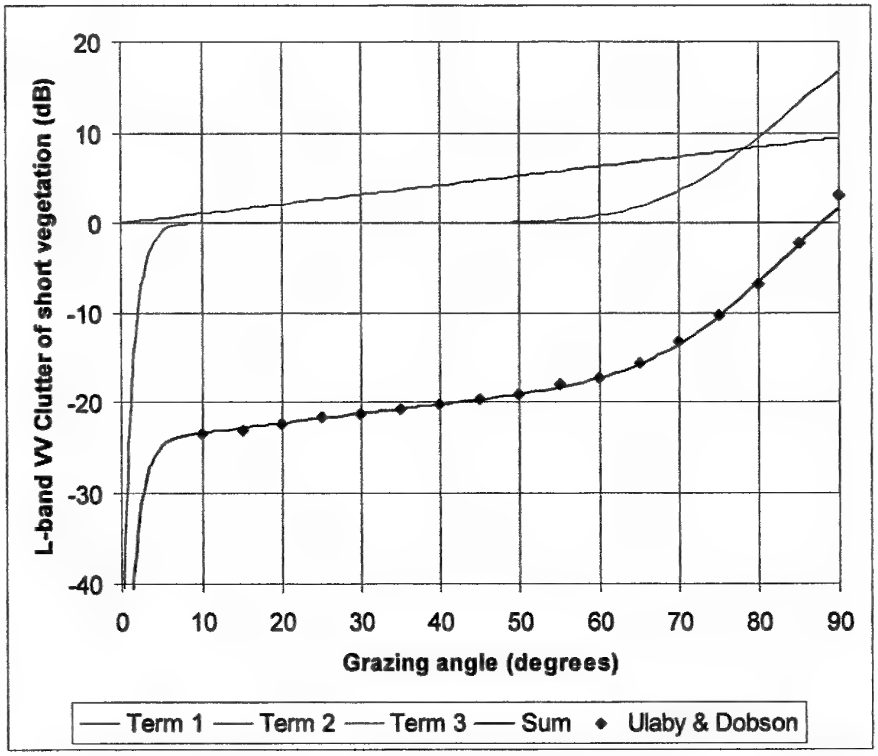

Figure 20: L-band VV clutter of short vegetation compiled by Ulaby and Dobson (1989) and its regression using the three-term model.

4.3 Typical Parameters of Land Clutter

The previous section has demonstrated that the proposed three-term clutter model is flexible and able to cope with various situations. This section will present typical parameters for various types of landcover, dedicated to L-band VV clutter.

4.3.1 AirSAR Measurements

AirSAR data for areas in the NT region have been collected and processed by NASA/JPL. The data have been used for clutter analysis, and details have been reported (Dong, 2003). In the analysis, SAR images are first segmented. The segments are then classified with the assistance of vegetation maps. The clutter distribution against grazing angle is obtained. Figure 21 shows L-band VV clutter measurements for bare soil (including the surface with little vegetation), grassland and eucalypt open woodland/forest. Measurements for grassland, shrub and short vegetation compiled from many sources by Ulaby and Dobson (1989) are also plotted in the figure for comparison. It can be seen that the consistency between AirSAR measurements and the

compiled measurements is very good. There is no compiled measurement data available for open woodland. But we know that the clutter difference between grassland and forests at L-band VV polarisation is about 7-10dB depending on tree height, density and biomass, we can be confident about the AirSAR measurement for the eucalypt open woodland. The AirSAR measurements for grazing angle beyond 70° however, seem incorrect, possibly due to the calibration errors for the near vertical incidence region.

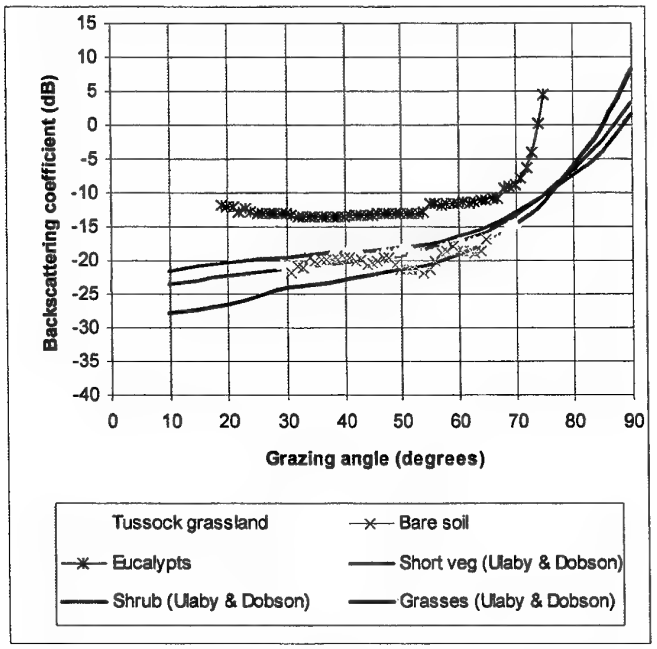

Figure 21: L-band VV clutter measurements for bare soil, grassland and eucalypt open woodland, together with measurements for grassland, shrub and short vegetation compiled by Ulaby and Dobson (1989).

The correlation between forest biomass and clutter value has been shown in Figure 12 where we can see that the clutter value generally increases with increases in biomass. Figure 22 shows the AirSAR measurements for eucalypt open woodland from four different sites. The locations and acquisition dates for these four sites are given in Table 2. Viewing measurements in Figure 22 and locations and acquisition dates in Table 2, we can conclude the measurements to be mainly correlated to biomass. The structure of trees should be similar, as they are the same species and in the same region, but the tree height and density are highly correlated to the precipitation. The lower clutter value for eucalypts in the Humpty Doo site, we believe, is because the trees are shorter and less dense resulting from a reduced annual precipitation for the site. Figure 22 also indicates that for forests at L-band, the effect of dry/wet season to clutter measurements is not so significant as we discussed for bare soil (see Section 3.2). A possible interpretation is given below. Woody parts of forests are the dominant

scatterers at L-band. In wet seasons, although the leafy mass of trees and the understorey vegetation increase, which increase the backscatter, the increase of the leafy mass also increases the attenuation effect. The total effect on backscatter of forests therefore might become insignificant. In fact we can see in Figure 7, unlike the clutter of bare soil, the variation of clutter of forests due to season changes is small even at C-band.

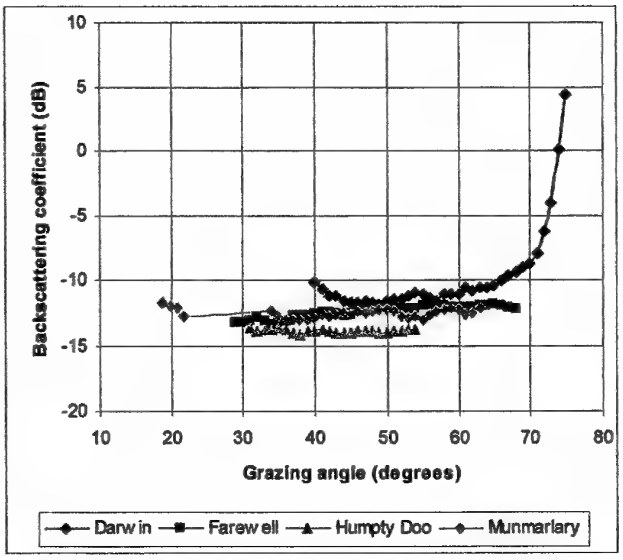

Figure 22:L-band VV Measurements of eucalypt open woodland in four different locations.

Table 2: Location and acquisition season of the four sites.

Site	Latitude	Location	Acquisition date / Season
Darwin	12.5°N	Close to sea	15/9/00; End of dry season
Farewell	12.0°N	Close to gulf	22/11/96; Start of wet season
Munmarlary	12.4°N	Not far from gulf	24/9/93; End of dry season
Humpty Doo	12.7°N	Inland	23/11/96; Start of wet season

The correlation of clutter to forest biomass as well as surface conditions can also be inferred from Figure 23 where measurements of various vegetations are shown. For instance, the measurement of melaleuca with free water on the surface (wet melaleuca) is about 4dB higher than the measurement of melaleuca without free water on the surface (dry melaleuca). Similarly, the measurement of waterfront mangrove is about 3-4dB higher than the measurement of other mangrove. In these two cases, the higher value is due to the water surface which enhances the double bounce scattering component. The clutter difference between patches of eucalypts and sparse eucalypts can be as great as 4-5dB.

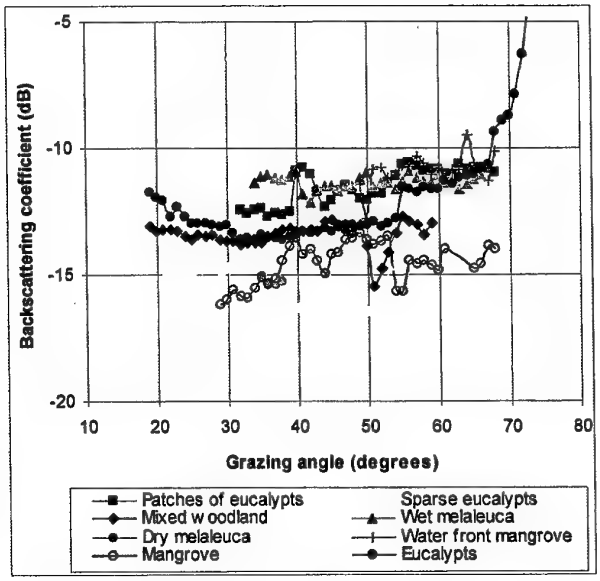

Figure 23:L-band VV Measurements of various vegetations.

Another observation from AirSAR measurements is that the L-band VV clutter value for a vegetation class at the plateau region remains approximately constant, i.e., the value is almost independent of grazing angle in this region. This can be seen in Figures 20-22. A perfect example is shown in Figure 24 where clutter levels out in the region of grazing angles from 30 to 55°.

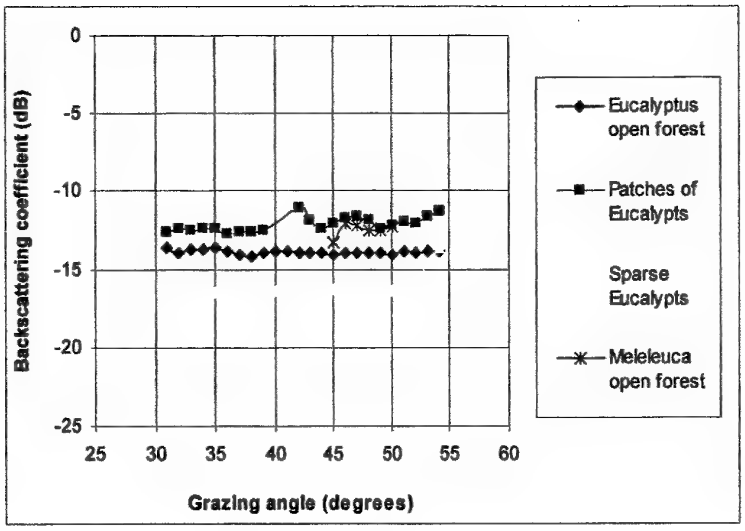

Figure 24: Clutter levels out for each class of vegetation in the plateau region.

4.3.2 Parameters

Because the AirSAR data do not cover the whole grazing angle region from 0 to 90 degrees, nor does the available data from the literature, we use the following principles to regress parameters:

- Using the MCARM data to determine the pattern of the curve in the low grazing incidence region;
- Using the AirSAR data to determine the pattern and the value of the curve in the plateau region;
- Using the compiled data by Ulaby and Dobson (1989) to determine the pattern and the value of the curve in the near vertical incidence region.

4.3.2.1 Open Woodland / Forest

About 40% of native vegetation in NT is open woodland / forest (DIPE 2002). According to AirSAR measurements, the clutter of open woodland / forest in the plateau region can vary about 5dB, from as low as -16dB to as high as -11dB depending on the biomass of forests as well as surface conditions. Instead of giving a single curve, we provide a band to cover the variation. Due to the evidence that the percentage of canopy closure is low for open woodland and that facets scattering will dominate at near vertical incidence, we assume the behaviour and value of clutter of open woodland to follow the pattern and value of short vegetation and shrub compiled by Ulaby and Dobson (1989). Table 3 lists the regressed parameters and their interpretations. The regressed curves are shown in Figure 25, in which the AirSAR

measurements for various open woodland and mangrove shown in Figure 23 are also re-plotted for comparison.

Table 3: Regressed parameters for open woodland and mangrove at L-band VV polarisation.

Region	Parameters	Meanings
Near grazing incidence	$c_1 = 50$ $k_1 = 45$	Value drops 1dB, 23dB and 46dB at 5°, 1° and 0.1°, respectively (see Figure 18).
Plateau region	$k2 = 2$	The linear increment is 2.1dB in the region of 5-65°.
Near vertical incidence	$k_3 = 0.9$ $c_3 = 16$ (22) $\eta = 20$	Follows the similar pattern and achieves the same value at 90° as compiled by Ulaby and Dobson for short vegetation. The value in the brackets is for the lower curve.
Level adjustment	$c_0 = -12.6$ (−17.6)	The value at the 45° is -11 (-16) dB.

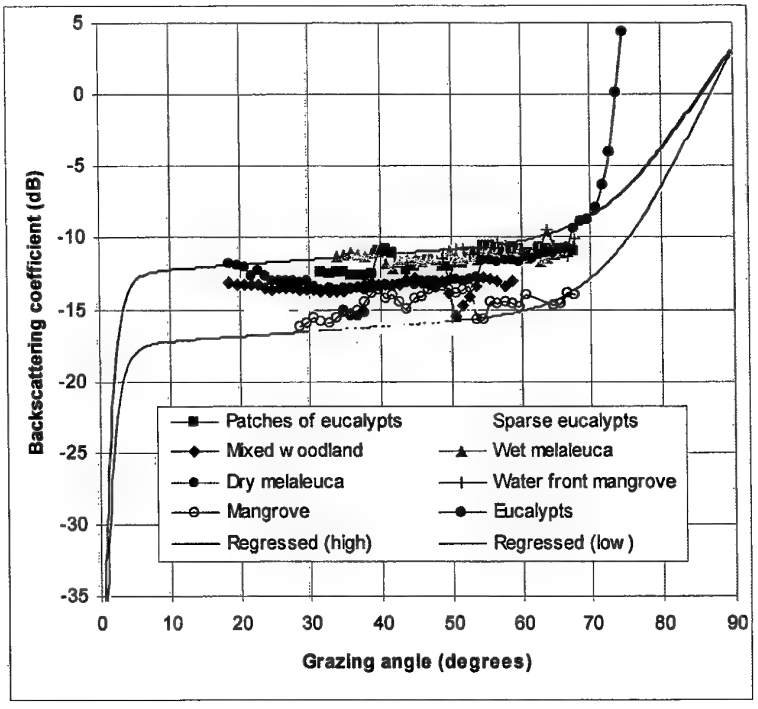

Figure 25: Regressed clutter of open woodland and mangrove with superposition of AirSAR measurements for open woodland and mangrove.

4.3.2.2 *Mangrove*

Over 4000 km^2 of mangroves are found along the NT coastline (DIPE 2002). The structure of mangrove is different from the structure of eucalyptus, one dominant species in open woodland / forest. Mangroves have very dense leafy material, but shorter and usually tilted trunks. They are commonly found in littoral areas in the top end of the NT. The L-band VV clutter of mangroves is, however, similar to the clutter of open woodland as shown in Figure 25, with waterfront mangrove at the top of the band and other mangroves close to the bottom of the band.

4.3.2.3 *Grassland and Bare Soil*

About 50% or more native vegetation in NT is grassland (DIPE 2002). According to the AirSAR measurement, the clutter of bare soil (with little vegetation) is close to the clutter of the grassland at L-band VV polarisation (Dong, 2003). This is because both volume scattering and volume attenuation at L-band are insignificant, so the grass layer is almost transparent to L-band and higher wavelengths. The dependence of clutter of bare soil on grazing angle has been described in Section 3.1. As shown in Figure 4, surface roughness plays a major role. The surface roughness in the NT region has not been measured, but the AirSAR measurement for the bare soil and grassland in the region at L-band VV polarisation shows little dependence on the grazing angle in the plateau region (Dong 2003), indicating that the surface is statistically rough at L-band. The regressed parameters for bare soil and grassland at L-band VV polarisation are given in Table 4. The regressed L-band VV clutter of bare soil and grassland is shown in Figure 26. The AirSAR measurements and the measurements compiled by Ulaby and Dobson are also plotted in the figure for comparison. The slope of the regressed curve at the plateau region is less than that of the compiled data. As we know, the slope is highly correlated to the surface roughness. The smoother the surface is, the sharper is the slope.

Table 4: Regressed parameters for bare soil and grassland at L-band VV polarisation.

Region	Parameters	Meanings
Near grazing incidence	$c_1 = 50$ $k_1 = 45$	Value drops 1dB, 23dB and 46dB at 5°, 1° and 0.1°, respectively (see Figure 18).
Plateau region	$k2 = 4$	The linear increment is 4.2dB in the region of 5-65°.
Near vertical incidence	$k_3 = 0.9$ $c_3 = 32$ $\eta = 20$	Follows the similar pattern and achieves the same value at 90° as compiled by Ulaby and Dobson for grassland.
Level adjustment	$c_0 = -23.1$	The value at the 45° is -20dB.

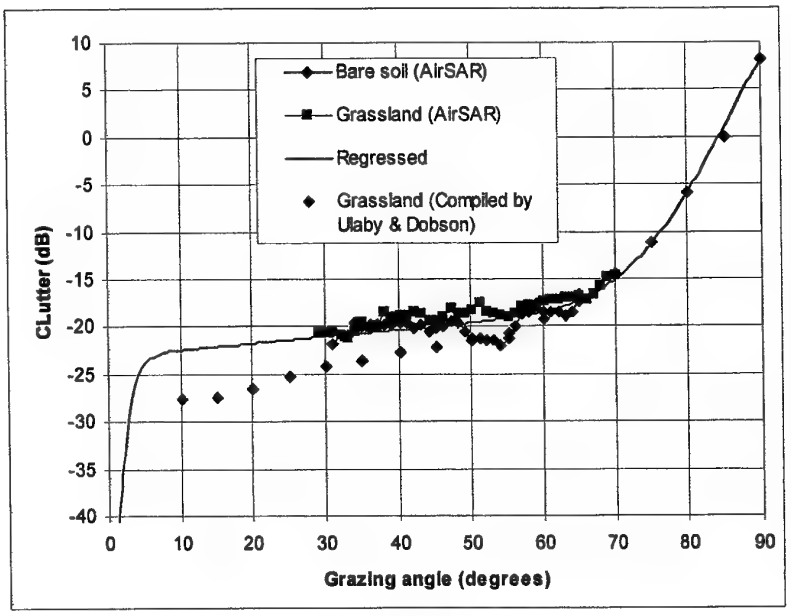

Figure 26: The regressed L-band VV clutter for bare soil and grassland. AirSAR measurements and the measurements compiled by Ulaby and Dobson (1989) are also shown for comparison.

4.3.2.4 Shrub and Short Vegetation

About 10% of native vegetation in the NT region belongs to the shrub category. Unfortunately, there are no reliable AirSAR measurements to support this category. In the Darwin scene, we measured the clutter of samphire shrub (Dong, 2003), but we believe the value was a few dB higher than it should be, possibly due to the presence of free water on the surface. According to the understanding of L-band clutter, the clutter of shrub and short vegetation should be between the clutter of bare soil and the clutter of open woodland, i.e., a few dB higher than the clutter of bare soil (assuming the surface roughness to be in the same order), but also a few dB lower than the clutter of open woodland. Accordingly with reference to the compiled data given by Ulaby and Dobson (1989) we expect the parameters for the L-band VV clutter of shrub and short vegetation to be very close to those given in Table 5. The regressed L-band VV clutter of shrub and short vegetation is plotted in Figure 27.

Table 5 Regressed parameters for shrub and short vegetation.

Region	Parameters	Meanings
Near grazing incidence	$c_1 = 50$ $k_1 = 45$	Value drops 1dB, 23dB and 46dB at 5°, 1° and 0.1°, respectively (see Figure 18).
Plateau region	$k2 = 4$	The linear increment is 4.2dB in the region of 5-65°.
Near vertical incidence	$k_3 = 0.95$ $c_3 = 18$ $\eta = 20$	Follows the similar pattern and achieves the same value at 90° as compiled by Ulaby and Dobson for shrub.
Level adjustment	$c_0 = -21.7$	The value at the 45° is -17.5dB.

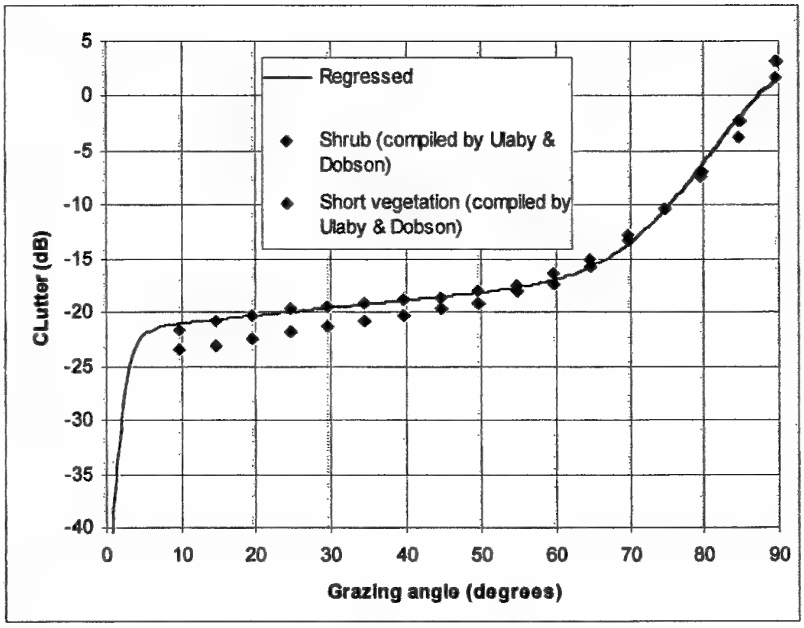

Figure 27: The regressed L-band VV clutter of shrub and short vegetation. The measurements compiled by Ulaby and Dobson (1989) are also shown.

4.3.2.5 Calm water

Lagoons and small lakes usually have a much smoother surface than the sea. Rivers in the Darwin area are also usually very calm because of the flat topography. The turbulence of the water due to tidal variations and wind is therefore several orders smaller than the turbulence of open seawater. It has been measured that the clutter from calm river water is typically 10-15dB below the clutter of bare soil (Dong 2003). The measured clutter of a flat river under the wind condition of sea state 2 is comparable to about sea clutter under the wind condition of sea state 0. It is expected that the clutter of lagoons and small lakes would behave similarly. The regressed

parameters for the clutter of calm water (seawater under the wind condition of sea state 0) are given in Table 6. The corresponding dependence of clutter on grazing angle is plotted in Figure 28, in which the AirSAR measurement of the South Alligator River is also plotted for comparison.

Table 6: The regressed parameters for L-band VV clutter of calm water

Region	Parameters	Meanings
Near grazing incidence	$c_1 = 42$ $k_1 = 35$	Values drops 2.0dB, 23dB and 36dB at 5°, 1° and 0.3°, respectively (Nathanson et al (1999).
Plateau region	$k2 = 12$	The linear increment is 10.5dB in the region of 10-60°.
Near vertical incidence	$k_3 = 0.95$ $c_3 = 51$ $\eta = 20$	Follows the similar pattern as compiled by Nathanson et al (1999) and achieves +20dB at 90°.
Level adjustment	$c_0 = -47$	The value at the 45° is -37.5dB.

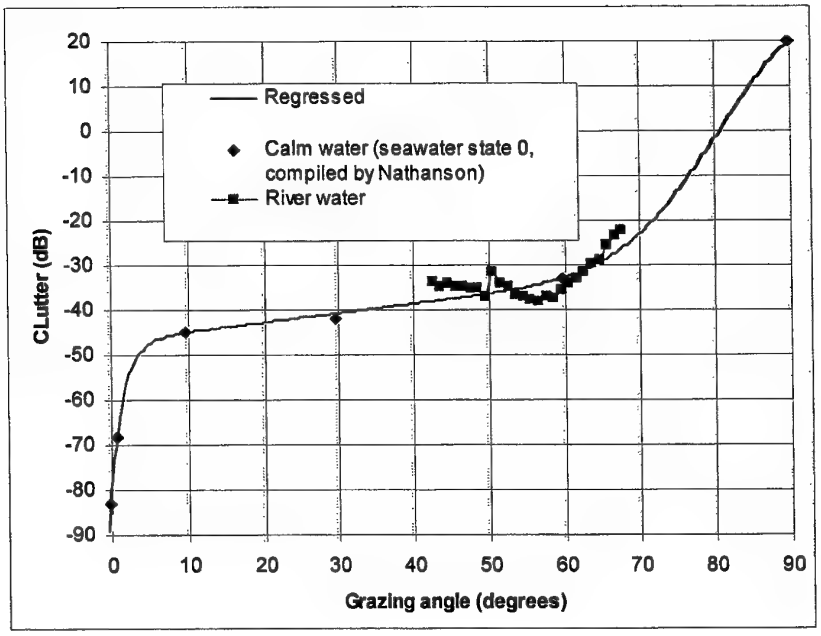

Figure 28: The regressed L-band VV clutter of calm water. The AirSAR measurement of the South Alligator River is also shown.

4.3.2.6 Urban Areas

Due to strong and discrete man-made scatterers, the variation in clutter of urban areas is usually much larger than that of natural surfaces. The amplitude of echo from urban

areas strongly depends on site conditions, including density, structure and orientation of house/building. Houses facing the radar produce strong corner-reflector-like returns, commonly known as the cardinal effect. Residential houses in the Darwin area typically have 20-35° tilted roofs and most are metallic. As a consequence, strong radar returns dominated by facet scattering can be measured at incidence angles close to the tilted angles of roofs. In general the clutter coefficients of urban areas are higher and the variation larger than that of vegetated areas (e.g., urban areas are normally brighter and spikier in SAR images). In the situation where suburbs are far away from the CBD (central business district) and houses are sparse, then the mean clutter should be approximately the same as the clutter of the vegetated surroundings. Figure 29 (a) shows an AirSAR L-band VV image of the Darwin area. The non-metropolitan areas are masked as shown in Figure 29 (b) in order to measure the clutter of the urban areas. The measured clutter is shown in Figure 30 together with comparisons of other measurements compiled by Ulaby and Dobson (1989), as well as Nathanson et al. (1999). It can be seen that the AirSAR measurement is higher than the compiled results. At this stage, it is felt that there are not sufficient data to regress the parameters for this category.

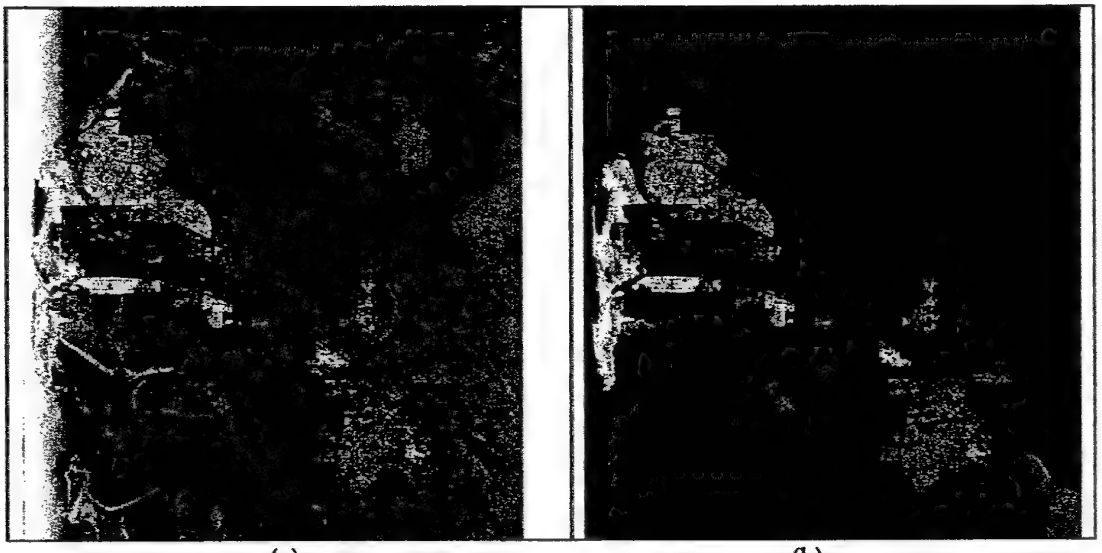

Figure 29: (a) An AirSAR L-VV image of the Darwin area and (b) the urban areas only. Images are in the slant range (near slant range at left and far slant range right), so distortions may be identified when compared with maps.

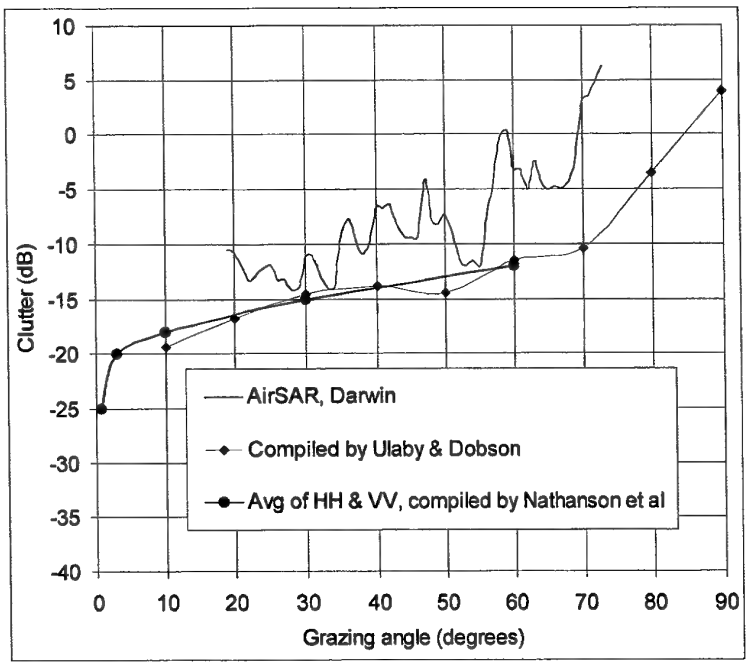

Figure 30: L-band VV clutter of urban areas measured from the AirSAR with compassions of the compiled data.

5. Clutter Spatial Distribution

Clutter values presented in Section 4 are mean values. Since clutter deals with scatterers randomly distributed in space, the measured clutter varies depending on the relative positions of individual scatterers. The resultant clutter is therefore a random variable. The clutter spatial distribution addresses the distribution of clutter given the same radar parameters, illumination geometry and the statistically same clutter environment.

5.1 Distribution Functions

It is well known that if there are many scatterers of approximately equal amplitude randomly distributed in illuminated patches, the distribution of clutter obeys Rayleigh statistics. In general, if a radar looks at a natural surface with a low resolution and at a not very low grazing angle (no dominant shadowing and multipath effects), the resultant clutter distribution is or is very close to Rayleigh. Modern radars often have high and very high resolutions, and/or illuminated areas often contain discrete man-made scatterers, and so the resultant distribution is usually much wider than the Rayleigh distribution. Clutter at low grazing angles does not obey the Rayleigh distribution because of the effects of shadowing and multipath propagation. In general

the Weibull, K- and lognormal distributions are most commonly used to approximate clutter spatial distribution (the Rayleigh distribution is a special case of both the Weibull and K- distributions). A detailed study of the clutter spatial distribution has been reported (Dong, 2004).

The probability density functions (pdfs) of the Weibull distribution in the linear domain and the dB domain, respectively, are,

$$p(x) = bcx^{b-1}\exp(-cx^b) \qquad x > 0 \tag{19}$$

$$p(z) = \frac{1}{k_0} bc\left(10^{z/10}\right)^b \exp\left(-c\left(10^{z/10}\right)^b\right) \tag{20}$$

where $a = 1/b$ and c are often referred to as the Weibull shape and scale parameters; $z = 10\log(x)$ and $k_0 = 10/\ln 10$.

The pdfs of the K-distribution in the linear domain and the dB domain, respectively, are,

$$p(x) = \frac{2\alpha}{\Gamma(\alpha)\bar{x}}\left(\frac{\alpha x}{\bar{x}}\right)^{\frac{\alpha-1}{2}} K_{\alpha-1}\left(2\sqrt{\frac{\alpha x}{\bar{x}}}\right) \qquad x > 0 \tag{21}$$

$$p(z) = \frac{1}{k_0}\frac{2}{\Gamma(\alpha)}\left(\frac{\alpha}{\bar{x}}10^{z/10}\right)^{\frac{\alpha+1}{2}} K_{\alpha-1}\left(2\sqrt{\frac{\alpha}{\bar{x}}10^{z/10}}\right) \tag{22}$$

where α is the shape parameter, $\bar{x}$ the mean of x and $K_v(\cdot)$ the modified Bessel function of the second kind.

The distribution of a random variable x is lognormal, if $\ln x$ is normally distributed with mean μ and variance s^2. The pdfs of the lognormal distribution in the linear domain and the dB domain, respectively, are,

$$p(x) = \frac{1}{\sqrt{2\pi}s}\frac{1}{x}\exp\left(-\frac{1}{2s^2}(\ln x - \mu)^2\right) \qquad x > 0 \tag{23}$$

$$p(z) = \frac{1}{k_0}\frac{1}{\sqrt{2\pi}s}\exp\left(-\frac{1}{2s^2}\left(\frac{z}{k_0} - \mu\right)^2\right) \tag{24}$$

5.1.1 Distribution of Homogeneous Clutter

Figure 31 shows the pdf of the low resolution MCARM L-band VV clutter of farmland. Due to the lack of calibration information, the mean has been normalised to 1 (0dB). Using the maximum likelihood (ML) estimation method, the parameters for both the Weibull and K- distributions have been obtained, and both are nearly identical to Rayleigh statistics as expected for a low resolution observation. The pdf of the data together with the estimated pdfs of the Weibull and K- distributions are shown in Figure 31. It can be seen that the difference between the two estimated distributions is very small. The parameters of the Weibull distribution in this case are $a = 0.9916$ (the Rayleigh distribution corresponds to $a = 1$) and $c = 0.9963$. The parameters of K-distribution are $\bar{x} = 1$ and $\alpha = 25.5876$ (the Rayleigh distribution corresponds to $\alpha = \infty$, and numerically $\alpha > 25$ can be considered as $\alpha = \infty$). Pdfs in the log scale are also plotted in the figure for viewing details of the distributions at the low probability ends.

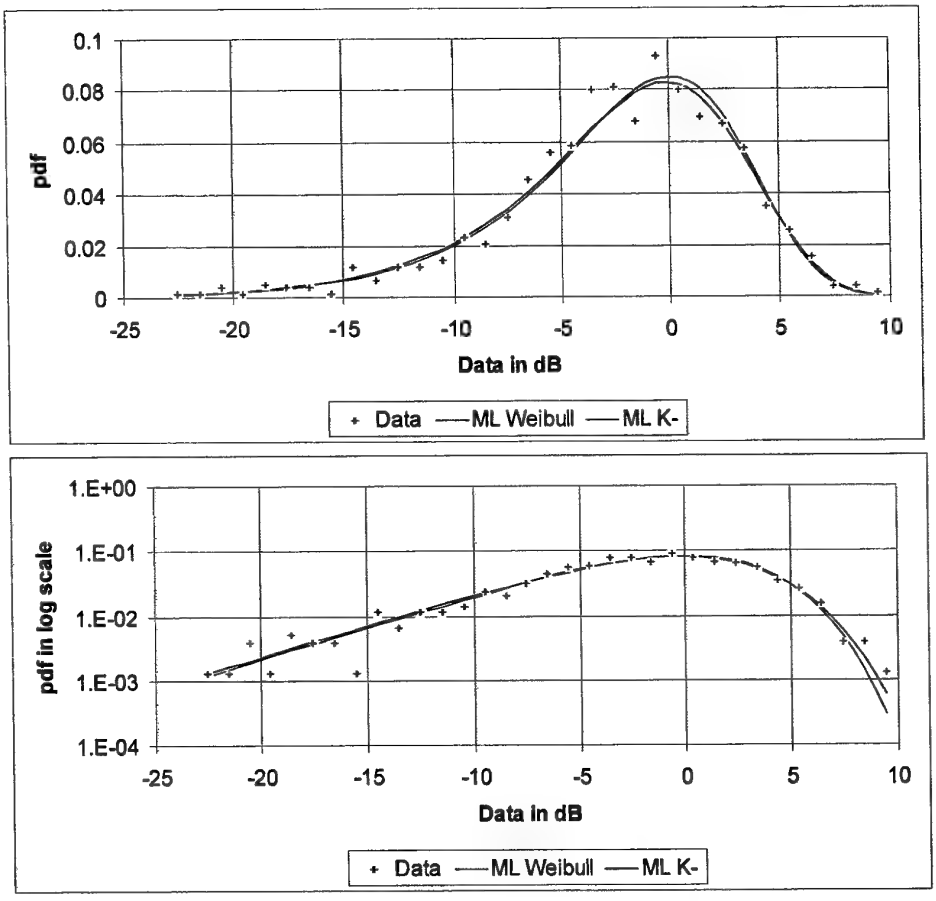

Figure 31: Spatial distribution of RAR L-band VV clutter of farmland. Pdfs in the log scale are also plotted for viewing details of the distribution at the low probability ends.

SAR synthesises RAR, so the distribution of single look SAR data can be considered as the distribution of RAR data assuming both SAR and RAR having the same parameters. Figure 32 shows the pdf of the AirSAR L-band VV single-look data of eucalypt open forest. The estimated Weibull and K- distributions for the data are also plotted in the figure. Pdfs are also plotted in the log scale for viewing details of the distributions at the low probability ends. The parameters obtained using the ML method are $a = 1.0243$ and $c = 2.4536$ for the Weibull distribution, and $\bar{x} = 0.4030$ and $\alpha = 23.7554$ for the K- distribution. Again the distributions are very close to the Raleigh distribution.

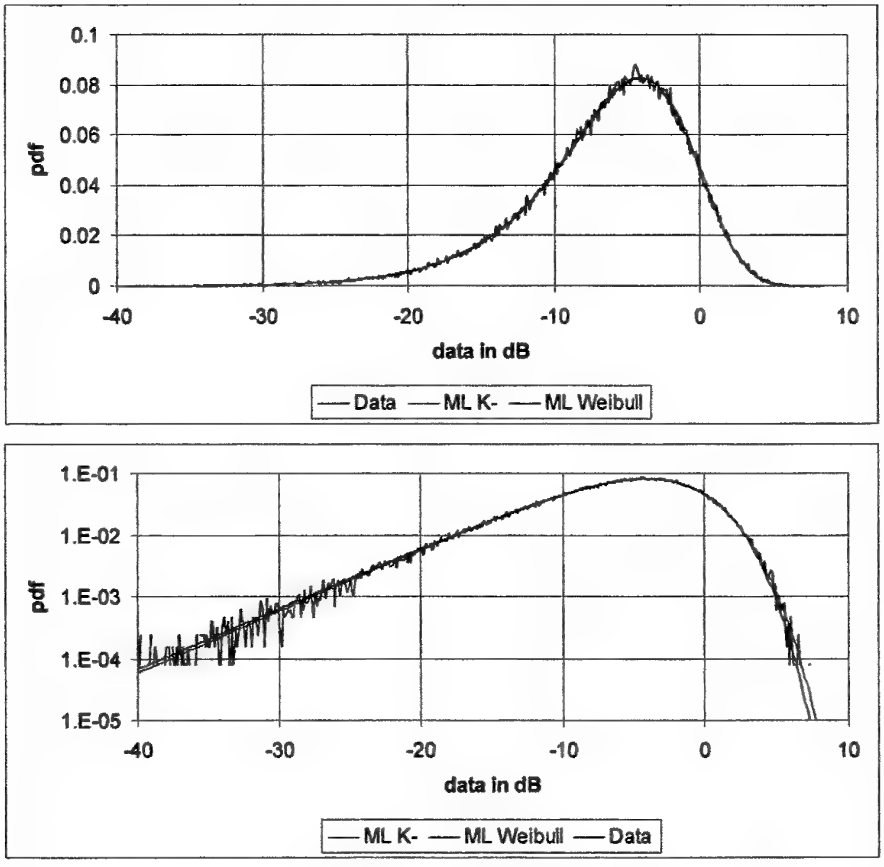

Figure 32: Spatial distribution of SAR L-band VV data of eucalypt open forest. Pdfs are also plotted in the log scale for viewing details of the distributions at the low probability ends.

5.1.2 Distribution of Heterogeneous Clutter

A heterogeneous area here means that some illuminated patches are statistically different from some other patches. For instance when a radar scans an area consisting of grassland and forest, the distribution of the clutter can be considered as a

combination of the clutter of grassland and the clutter of forest. Supposing there are n different types of landcover, and the clutter of each of them is a Rayleigh, the combined distribution is,

$$p(x) = \sum_{i=1}^{n} k_i p_i(x;\bar{x}_i) \tag{25}$$

where $p_i(x;\bar{x}_i)$ is the pdf of Rayleigh with mean $\bar{x}_i$, k_i is the portion of *ith* type of landcover, and $k_1 + \cdots + k_n = 1$.

If we prefer to use a single Weibull or K- distribution function to approximate the above distribution, we may use parameter estimation (this will be addressed in the following section) schemes to obtain parameters for the distribution.

As an example, in Figure 33 we assumed that a heterogenous area comprises 70% of open forest with a mean clutter of –12dB and 30% of bare soil with a mean clutter of –18dB, and the clutter of each of them obeys Rayleigh statistics. It is obvious from the figure that the combined clutter distribution is broader than a Rayleigh and may be approximated by a Weibull or K- distribution. The corresponding clutter parameters for forest, bare soil and the combined are given in Table 7. The approximated Weibull and K- distributions for the combined distribution are shown in Figure 34 and Figure 35, respectively. It can be seen that the combined distribution is not a perfect Weibull or K- distribution. In this case, the Weibull apprximation results in some errors in the low to mid-value range, while the convergence of the K- approximation is slower that the convergence of the combined data. We have also tried some other different combinations, and the errors of the approximations are similar.

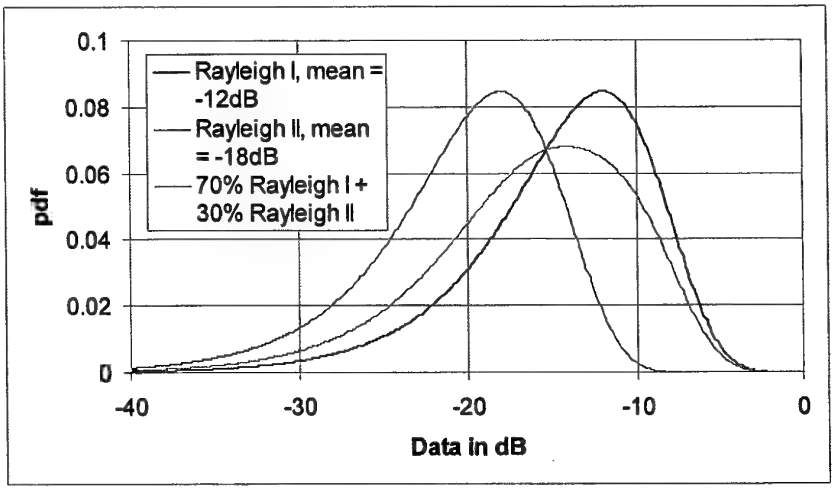

Figure 33: A combined distribution of two Rayleigh distributions is generally a non-Rayleigh.

Table 7: Parameters of the combined clutter comprising 70% forest and 30% bare soil.

	Weibull parameters	K- parameters
Clutter of forest	$a=1;\ c=15.8489$	$\bar{x}=0.06310;\ \alpha=\infty$
Clutter of bare soil	$a=1;\ c=63.0957$	$\bar{x}=0.01585;\ \alpha=\infty$
Combined clutter	$a=1.1527;\ c=14.5859$	$\bar{x}=0.04892;\ \alpha=3.2815$

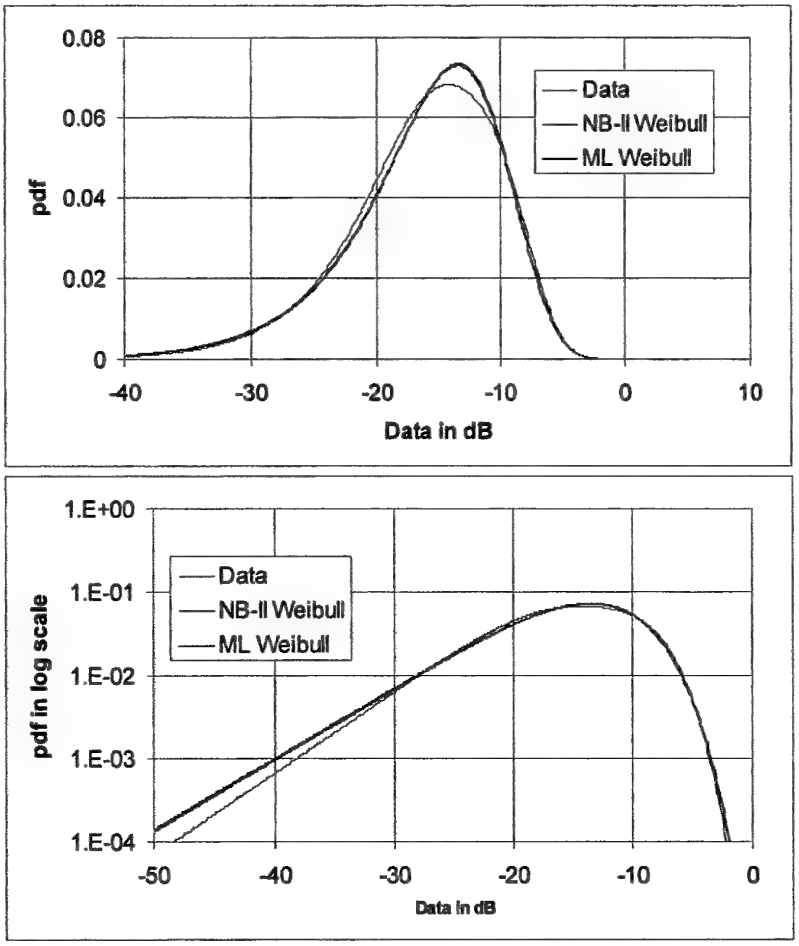

Figure 34:The Weibull distribution is used to approximate a combination of two Rayleigh distributions. The pdfs are also plotted in the log scale for a detail view of the low probability ends.

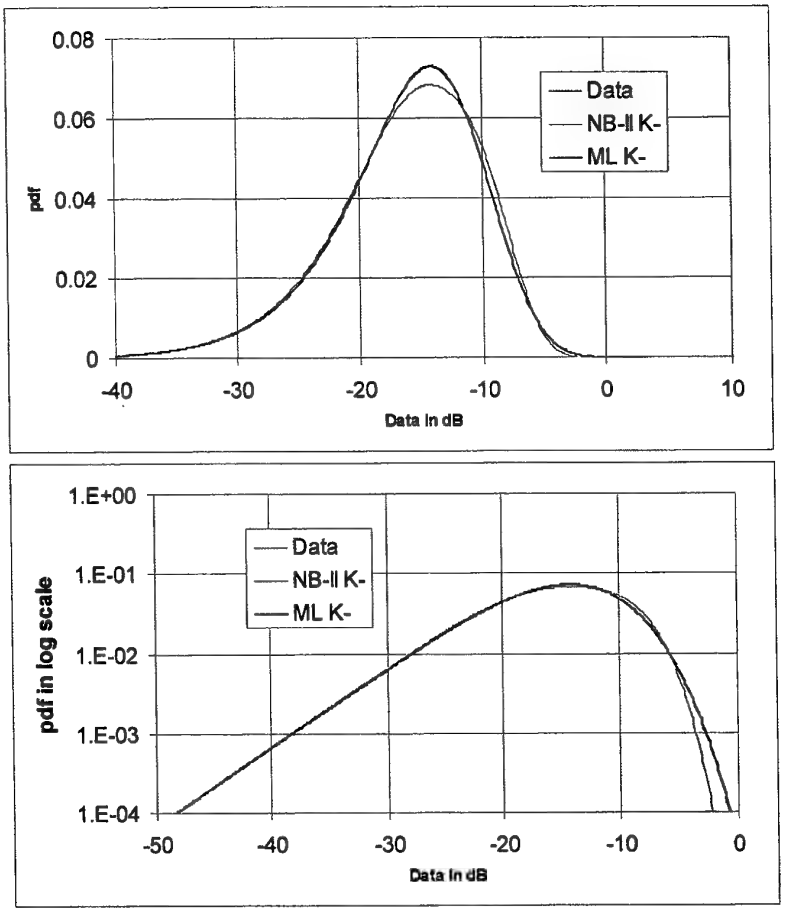

Figure 35: The K- distribution is used to approximate a combination of two Rayleigh distributions. The pdfs are also plotted in the log scale for a detail view of the low probability ends.

5.1.3 Distribution of High Resolution and Low Grazing Angle Data

Clutter collected at high resolution is not well developed, i.e., scatterers vary from cell to cell and cannot be considered as statistically homogenous. Effects of shadowing and multipath propagation are becoming dominant at low grazing angles. All these violate the criterion of the Rayleigh distribution. A case of the clutter distribution approximately obeying the lognormal distribution is shown in Figure 36. It is the RAR X-band VV clutter of seawater. The radar's range resolution is high (0.3 m) and grazing angle low (approximate 0°). Viewing the figure carefully, we can see that the distribution is not quite a lognormal distribution. The peak of the estimated distribution is lower than the peak of the data distribution, while the chest of the

estimated distribution is higher than the chest of the data distribution. But among the three commonly used distribution models, the lognormal distribution is the best approximation to the data distribution in this case.

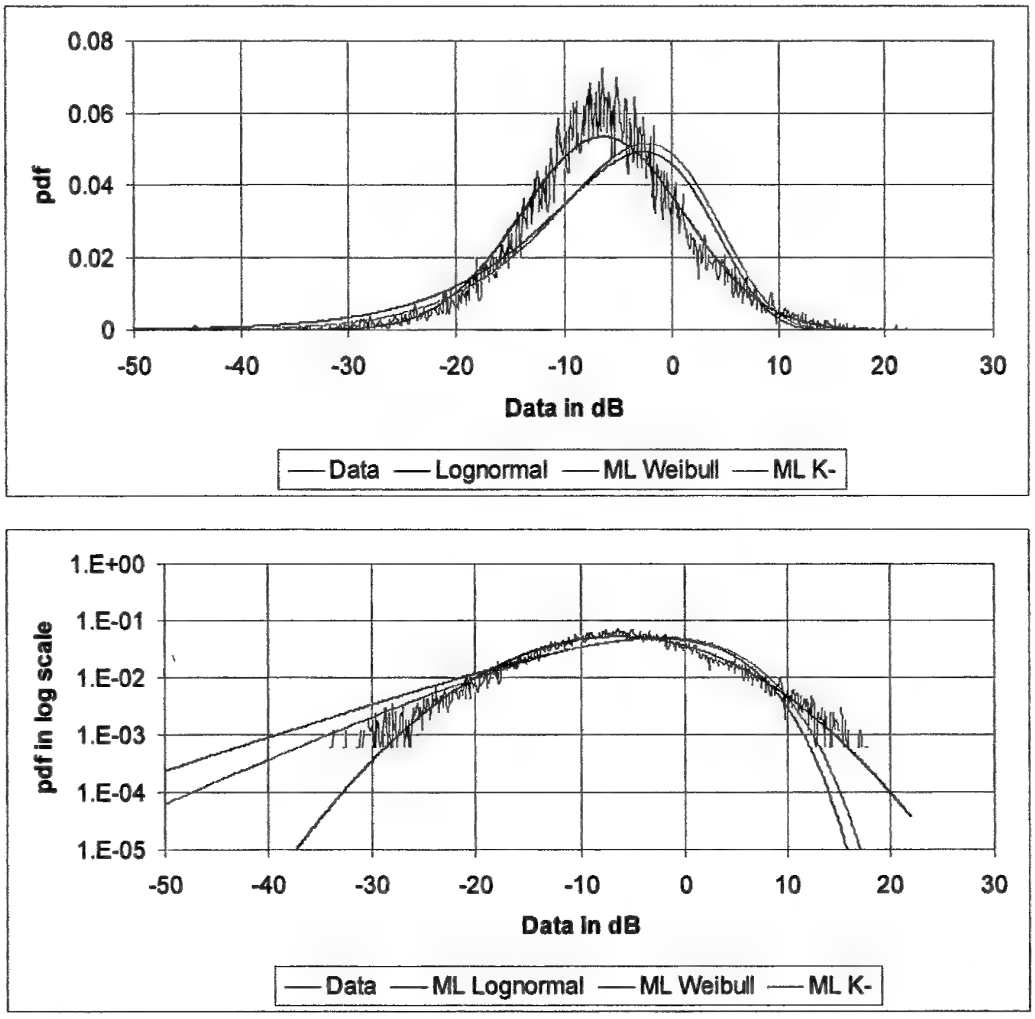

Figure 36: The pdf of sea clutter as well as its ML Weibull, K- and lognormal distributions. The data were RAR X-band VV polarisation with high resolution (0.3 m in range) and low grazing angle (approximate 0°). Pdfs in the log scale are also plotted for a detail view of the low probability ends.

5.2 Parameter Estimation for Distribution Functions

The Weibull, K- and lognormal distributions are commonly used to approximate clutter spatial distribution. However, in addition to the varying mean, which

determines the position of the pdf, the shape parameter, which determines the broadness of the pdf, also varies. As a consequence, parameter estimation is often involved in determining distribution parameters for dedicated clutter data.

Theoretically the ML estimates are the optimal. In the case of the lognormal distribution, the ML estimates of two parameters μ and s are simply the mean and the standard deviation of the sample data presented in the natural logarithmic domain. Unfortunately for the Weibull and K- distributions, iterative algorithms manipulating sample data are involved in determining the ML estimates, which may not be desirable in real time implementation which requires simple and fast algorithms. A fast and simple estimation scheme, named as NB-II (no bias II) scheme has been proposed for parameter estimation for both the Weibull and K- distributions (Dong, 2004). The scheme provides estimates nearly identical to the ML estimates. It uses $E(x)$ (arithmetic mean) and $E(z) = E(10\log x)$ (geometric mean) to estimate parameters. Therefore the estimates are no bias in terms of $E(x)$ and $E(z)$. For the integrity of this report, we quote the ML and the NB-II schemes for both the Weibull and K- distributions below.

The ML estimates for the Weibull distribution can be determined using the iterative algorithm,

$$\begin{cases} \dfrac{1}{\hat{c}_k} = E\left(x^{\hat{b}_{k-1}}\right) \\ \dfrac{1}{\hat{b}_k} = \hat{c}_k E\left(x^{\hat{b}_{k-1}} y\right) - E(y) \end{cases} \qquad k = 1, 2, \cdots \tag{26}$$

Without losing generality, we can let $\hat{b}_0 = 1$. The iteration stops if $\left\|\hat{c}_k - \hat{c}_{k-1}\right\| < \varepsilon$, where ε is a given acceptable error. It is worth noting that the iteration of (26) involves sample data. Usually the number of sample data is large in order to obtain a reliable distribution, so the algorithm is slow.

Alternatively, the NB-II estimates for the Weibull distribution can be determined by,

$$\begin{cases} \ln\Gamma(1+\hat{a}) + \dfrac{E(z)}{k_0} + \hat{a}\gamma - \ln E(x) = 0 \\ \hat{c} = \exp\left(-\dfrac{E(z)}{k_0 \hat{a}} - \gamma\right) \end{cases} \tag{27}$$

where $\gamma = -\psi^{(0)}(1) = 0.577215665$, is Euler's Gamma constant. The first equation of (27) is nonlinear, and an iterative technique might be sought to numerically determine the value of $\hat{a}$. But this iteration should be several orders faster than the iteration of the ML method, as the manipulation of sample data is not involved in the iteration.

The ML estimates and NB-II estimates for the K- distribution are given in (28) and (29), respectively. Similarly, the manipulation of sample data is involved in an iterative algorithm in computing the ML estimates, whereas the NB-II scheme only requires solving a nonlinear equation.

$$\begin{cases} \overline{x} = \dfrac{1}{n}\sum_{i=1}^{n} x_i = E(x) \\ \hat{\alpha} \Leftarrow \max\limits_{\alpha} \left\{ n\ln\alpha - n\ln\Gamma(a) + \dfrac{\alpha-1}{2}\left(n\ln\alpha - n\ln\overline{x} + \sum_{i=1}^{n}\ln x_i \right) + \sum_{i=1}^{n}\ln K_{\alpha-1}\left(2\sqrt{\dfrac{\alpha}{\overline{x}} x_i} \right) \right\} \end{cases} \tag{28}$$

$$\begin{cases} \overline{x} = E(x) \\ \psi^{(0)}(\hat{\alpha}) - \ln\hat{\alpha} = \gamma - \ln\overline{x} + \dfrac{1}{k_0} E(z) \end{cases} \tag{29}$$

where $\psi^{(n)}(x)$ is the Polygamma function, defined as the n^{th} derivative of the logarithm of the Gamma function, $\dfrac{d^{n+1}}{dx^{n+1}}(\ln\Gamma(x))$.

It has been found that the NB-II estimates are nearly identical to the ML estimates, so the NB-II scheme can be considered as an asymptote to the ML scheme that is the optimal. Distributions plotted by using the ML and NB-II estimates are shown in Figure 34 and Figure 35, and no noticeable difference between the two can be seen. More discussions and examples can be found elsewhere (Dong, 2004).

6. Clutter Temporal Distribution

Motion of moving parts, such as tree leaves and branches and sea waves, causes the clutter return to fluctuate with time. The variation of clutter with respect to time is referred to as the temporal variation in the time domain. The corresponding variation in the frequency domain is of more concern, as moving target indication (MTI) radar utilises Doppler processing to separate weak moving targets from strong clutter returns.

From the viewpoint of Doppler frequency shift, land scatterers can be grouped into two general categories: (1) those that move with wind and (2) those that do not move with wind, such as trunks, rocks, and the bare ground surface. If there are moving scatterers, such as grass, flowers, leaves, twigs and possibly branches, there are usually many within an illuminated area. Therefore, it seems that the moving scatterers should have electromagnetic properties similar to those of a large collection of random scatterers (Long, 2001), leading to the fluctuation of clutter return to be random in general. The Doppler frequency shift of clutter is frequency dependent. For instance, the phase variation of the backscattered electric field from a scatterer that is moving

back and forth one centimetre is large for millimetre wavelengths, but remains nearly constant for decimetre wavelengths.

The Doppler frequency of clutter at L-band is usually low and its amplitude quickly falls off exponentially to levels 60 to 80dB down from zero Doppler within a span of about ±10 Hz. The Doppler resolution of both the medium and low PRF MCARM data of the analogue sum channel in range-Doppler bins is low (15.5 Hz), so that the Doppler information contained in the range-Doppler bins is mainly generated by locations of scatterers rather than the motion of scatterers. In other words, we generally cannot extract Doppler spectra of clutter from processing the MCARM analogue sum channel data. The material of this Section is therefore mainly from Billingsley's work (2002).

Land clutter generally contains both a constant (or steady) component and a varying component corresponding to stationary and moving parts of clutter, respectively. The steady component gives rise to a DC or zero-Doppler term in the power spectrum of the returned signal, and the varying component gives rise to an AC term in the spectrum. Billingsley (2002) expresses the total spectral power density $P_t(v)$ as a sum of a DC term and an AC term,

$$P_t(v) = \frac{r}{1+r}\delta(v) + \frac{1}{1+r}P_{ac}(v) \tag{30}$$

where v is the Doppler velocity in m/s; r is the ratio of DC power to AC power of the spectrum; $\delta(v)$ is the Dirac delta function representing the DC component in the spectrum and $P_{av}(v)$ denote the AC component of the spectrum, normalised such that

$$\int_{-\infty}^{\infty} P_{ac}(v)dv = 1 \tag{31}$$

Also by definition,

$$\int_{-\infty}^{\infty} \delta(v)dv = 1 \tag{32}$$

It follows that the integral of $P_t(v)$ with respect to v is equal to unit:

$$\int_{-\infty}^{\infty} P_t(v)dv = 1 \tag{33}$$

The Doppler frequency shift f in hertz and Doppler velocity v in m/s are fundamentally related as

$$f = -\frac{2v}{\lambda} \tag{34}$$

6.1 AC Power Spectrum

Billingsley (2002) has found that the shape of the AC component of the clutter signal power spectrum is a two-sided exponentially decaying curve, and can be expressed as,

$$P_{ac}(v) = \frac{\beta}{2}\exp(-\beta|v|) \quad -\infty < v < \infty \tag{35}$$

where β is the exponential shape parameter[9]. It is a function of wind conditions. Table 8 provides values of the shape parameter as a function of wind speed. The exponential decay of the AC component of clutter Doppler spectra specified by (35) is plotted in Figure 37 using parameters given in Table 8. According to Billingsley (2002), the values of β in Table 8 are largely independent of radar frequency over range from VHF to X-band.

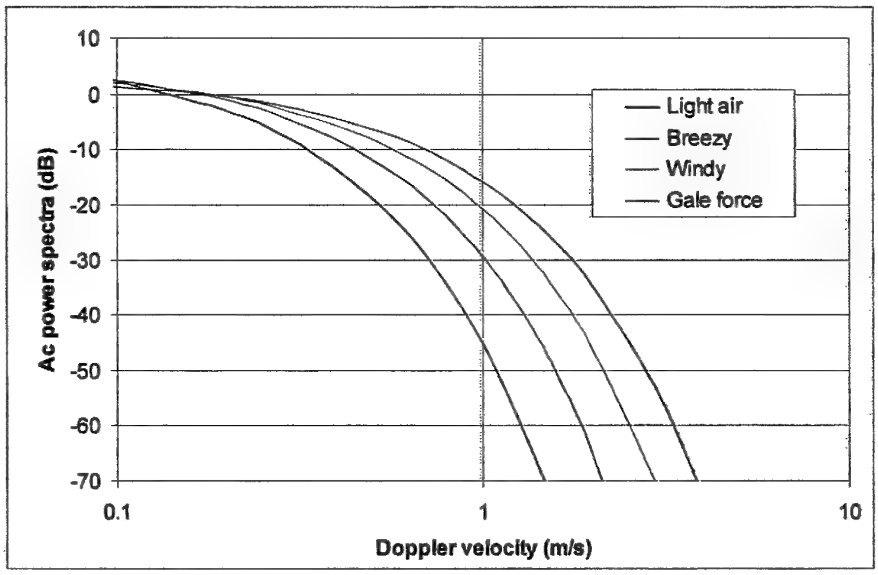

Figure 37: Exponential model for AC clutter spectra of windblown vegetation (Billingsley, 2002).

[9] β denotes grazing angle in Section 4.

Table 8: AC shape parameter β vs wind speed (Billingsley, 2002)

Wind conditions	Wind speed (mph[10])	Shape parameter β	
		Typical	Worst case
Light air	1-7	12	-
Breezy	7-15	8	-
Windy	15-30	5.7	5.2
Gale force	30-60	4.3	3.8

As indicated in (34), it follows immediately that the AC Doppler frequency spectrum due to motion of windblown vegetation is simply a linear scaling of the scatterer Doppler velocity as shown in Figure 37 with respect to radar frequency.

Shown in Figure 38 are measurements of AC components of forest clutter spectra under various wind conditions. The measurements were conducted by Billingsley (2002) using a conventional L-band analogue coherent radar. These measurements agree well with the exponential decay model of (35) and parameters in Table 8.

[10] Miles per hour, $1mph = 0.44694 m/s$.

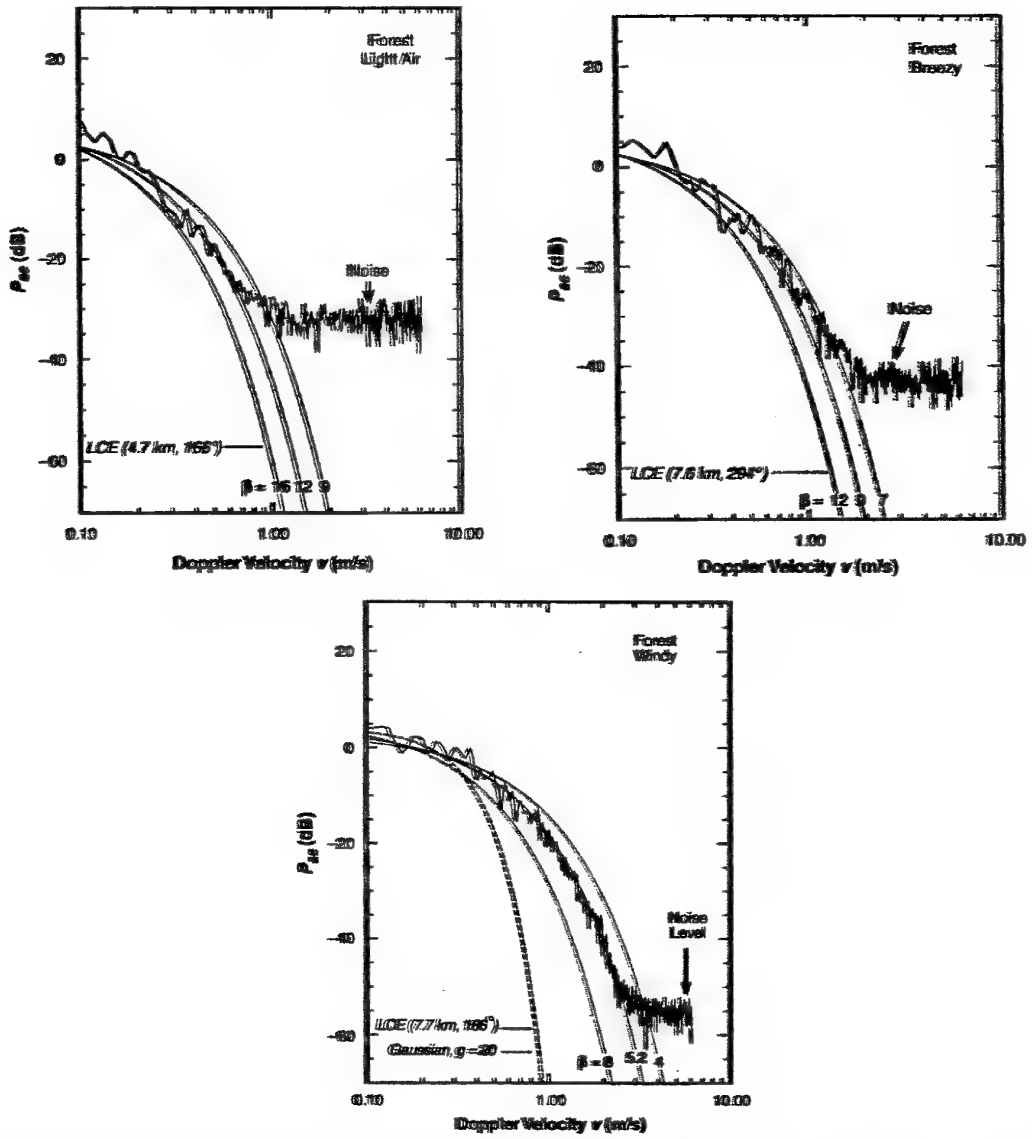

Figure 38: Exponential decay in AC components of forest clutter spectra measured under light air, breezy and windy conditions, respectively (Billingsley, 2002).

6.2 Ratio of DC/AC

Although the AC spectra of the Doppler velocity are largely independent of radar frequency, it is understandable that the ratio of DC/AC is strongly dependent on both wind speed and radar frequency. Billingsley (2002) gives the expression of r for windblown trees as,

$$r = 489.8 w^{-1.55} f^{-1.21} \quad (36)$$

where w is the wind speed in mph and f is the radar carrier frequency in gigahertz.

This statistical formula covers the frequency range from 170 MHz to 9.2 GHz. The variation of r with wind speed and radar frequency as specified in (36) is plotted in Figure 39. The quantity r is also the ratio of steady power to total random power as defined in (30). It can be seen that at L-band the DC component dominates for wind speeds up to 30 mph.

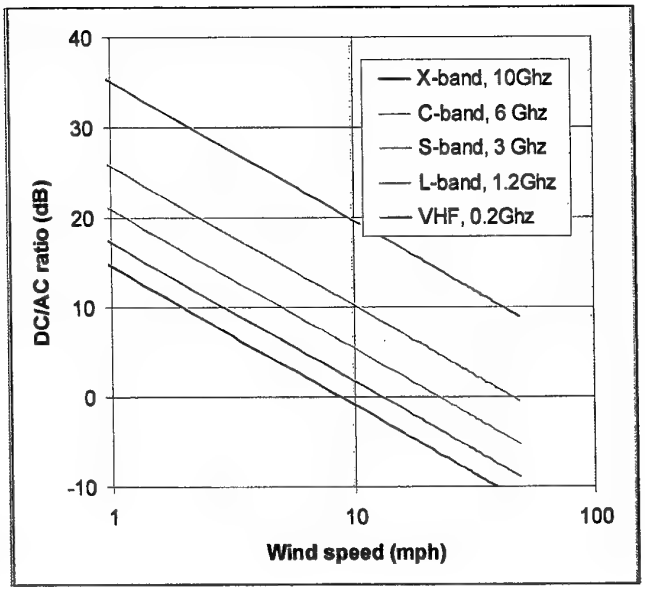

Figure 39: The ratio of DC to AC spectral power in windblown forest clutter spectra vs wind and radar frequency (Billingsley, 2002).

According to Billingsley (2002), except for wind speed and radar frequency, other parameters, including tree species, season of year, wind direction, polarisation, resolution, range, and depression/grazing angle appear to be largely subsumed within the general range of statistical variability of the measured data.

Values of r for a few typical land covers at L-band are listed in Table 9 (Billingsley, 2002).

The exponential model was explicitly derived to be applicable to windblown trees, but it can also perform adequately for other windblown vegetation types including shrub desert, cropland, grassland and rangeland, by suitably adjusting its DC/AC ratio. Figure 40 shows the comparison of AC spectral shapes of L-band clutter of desert

(shrub/bush) and forests under windy conditions. It can be seen that both follow the exponential decay model.

Table 9: Values of r for a few typical land covers at L-band (Billingsley, 2002)

Land cover category	Wind speed (mph)	Ratio of DC/AC (dB)	Description of site
Forest	10	10	Typical forest
Rangeland	Not specified	15-20	Patches of aspen trees of about 13m in height and patches of willow shrubs of 4.5m in height.
Farmland	14	21	Wheatfield in June (north hemisphere) with trees occurrence of 1-3%
Desert	20	24	Sparse desert bushes of about 1m in height.

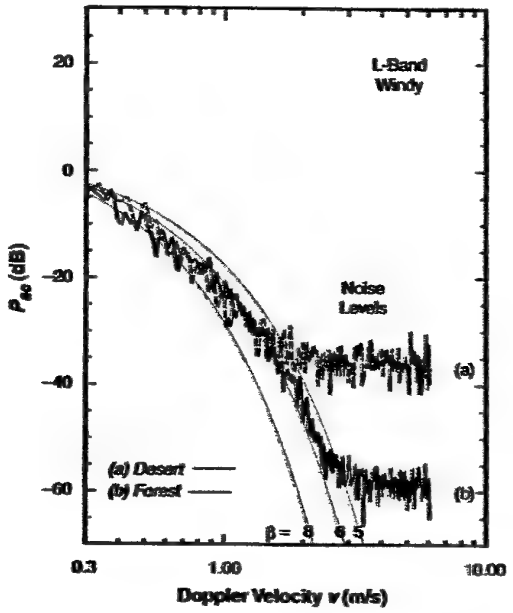

Figure 40: Comparison of AC spectral shapes of L-band clutter of (a) desert (shrub /bush) and (b) forests under windy conditions (Billingsley, 2002).

6.3 Fast and Slow Components of Spectrum

Helmken (1990) and Chan (1990) have observed sea clutter at low grazing angles with L, S and C band radars. Both have found the Doppler spectrum of sea clutter to contain twin peaks including a slow component (low frequency) and a fast component (high frequency). Helmken (1990) has found that the slow component moves at one-quarter

of the wind speed and is consistent with capillary wave motion. At the measured sea states of 3 and 5, the slow component dominates the total RCS to at least the range of the horizon, and decreases by an order of 15dB per range doubling. The fast component moves at the wind speed and is believed to be associated with clear air echoes caused by fluctuations of the refractive index of the atmosphere. The reflectivity of this fast component is nearly constant and extends in range far beyond the horizon.

6.4 Correlation Time for Windblown Trees

Correlation time is important to data collection and processing. It has been found that the correlation time for windblown trees is a function of frequency, the longer the wavelength, the longer the correlation time. The typical correlation time for clutter of windblown trees is given in Table 10.

Table 10: Typical correlation time for windblown trees (Billingsley, 2002)

Frequency band	VHF	UHF	L-band	S-band	X-band
Typical correlation time (s)	5.04	0.94	0.95	0.081	0.049

7. Summary

We have discussed and addressed land clutter, its associated issues and modelling. Although the discussion is mainly from a perspective of L-band VV polarisation, many concepts can be extended to other frequencies and polarisations. In particular this report has focused on the modelling of:

- Clutter distribution against grazing angle;
- Cutter spatial distribution; and
- Clutter temporal distribution (Doppler spectrum).

A three-term model for the dependence of clutter on grazing angle has been proposed. The three terms model clutter behaviour in the near grazing incidence, plateau and near vertical incidence regions, respectively. The model is supposed to be site-specific and landcover-dependent, i.e., parameters for different types of landcover are supposed to be different. Based on measurements of the AirSAR and MCARM systems, and measurements compiled by other researchers, parameters for dominant types of landcover in the Northern Territory region including eucalypt open woodland/forest, mangrove, shrub/short vegetation, grassland/bare soil and calm river water, have been regressed. Comparisons between the regressed curves and available measurements have shown good agreement.

Also discussed is clutter spatial distribution. For the same illumination geometry and a statistically homogeneous clutter environment, clutter echo obeys a random process because scatterers are randomly distributed in space. It has been found that the

distribution of low resolution clutter data of homogenous landcover is, or very close to, the Rayleigh distribution as supported by the theory. If each resolution cell contains only one type of landcover, but the radar scanning area has more than one type of landcover, then the clutter distribution can be considered as a combination of Rayleigh distributions with different means and different weights. The combined distribution may be approximated as the Weibull or K- distribution. Agreeing with others, we have also found that the distribution of seawater clutter acquired by a high resolution C-band VV radar at near zero degree grazing angle is approximately a lognormal distribution. A sea surface may be homogenous, but individual cells may not when the resolution is high, leading to the random process not being fully developed. Effects of shadowing and multipath propagation may become dominant at a low grazing angle. All these break the criterion of Rayleigh distribution.

The Weibull, K- and lognormal distributions are the most commonly used to approximate the spatial distribution of surface clutter. Depending on the data, one may be found better than the others for approximating the distribution. The Weibull and K-distributions are very similar and the differences between the two are small for those distributions whose shape parameter is not far from the Rayleigh distribution. The lognormal distribution is usually applied to high resolution and low grazing angle data collected from sea surfaces and areas containing strong discrete scatterers including buildings and other man-built targets. The lognormal distribution converges the slowest, which is sometimes referred to as having the longest tail.

Fast parameter estimation is an issue given a distribution model and sample data, if the estimation is to be implemented in real-time. Estimates obtained using the ML method are the optimal. Except for the lognormal distribution, the ML estimates for both the Weibull and K- distributions require an iterative algorithm manipulating sample data. The size of sample data sets is usually large in order to obtain reliable statistics, so the iterative algorithm is slow. A fast and simple parameter estimation scheme, named as NB-II, has been proposed. The NB-II estimation scheme uses the arithmetic mean and the geometric mean to estimate parameters, so the estimated distribution has no bias with respect to the arithmetic mean and the geometric mean of sample data. The NB-II estimates have been found to be nearly identical to the ML estimates, and can be considered as an asymptote to the ML estimates.

The clutter temporal distribution, or equivalently the Doppler spectrum caused by motion of moving parts of scatterers has also been discussed. The Doppler frequency of L-band land clutter is low and decays rapidly. We do not have proper measured data to investigate. The discussion has been mainly based on available materials from open literature. The main points of the distribution include (1) the Doppler velocity decays exponentially; (2) the shape parameter of the decay function is only dependent on wind conditions and largely independent of radar frequency; (3) the ratio of DC component to AC component of the Doppler spectrum depends on wind conditions, type of landcover and radar frequency but is largely independent of polarisation.

8. Acknowledgement

The author thanks Drs A Shaw and J Whitrow for their various technical comments, discussions and grammar corrections, and Mr S Capon for his administrative support. Thanks also go to the vetting officer, Dr P L Choong. The MCARM data were from the Rome Laboratory, Air Force Material Command, Rome, New York.

9. References

1. AUSLIG (Australian Surveying and Land Information Group), *Atlas of Australian Resources, Third Series*, Volume 6: *Vegetation*, Canberra, 1990.

2. Billingsley, J B, *Low-Angle Land Clutter Measurements and Empirical Models*, William Andrew Publishing, 2002.

3. Boyarskii, D A, Tikhonov, V V, and Komarova, N Y, "Model of dielectric constant of bound water soil for application of microwave remote sensing," PIERS, Vol 32, pp. 251-269, 2002.

4. Chan, H C, "Radar sea clutter at low grazing angles," *IEE Proceedings, Part F*, vol. 137, no. 2, pp. 102-112, 1990.

5. DIPE (Department of Infrastructure, Planning and Environment), the Northern Territory, *http://www.lpe.nt.gov.au*, 2002.

6. Dobson, M C, Ulaby, F T, Le Toan, T, Beaudoin, A, Kasischke, E S, and Christensen, N, "Dependence of radar scatter on coniferous forest biomass," *IEEE Trans on Geoscience and Remote Sensing*, vol . 30, no. 2, pp. 412-415, 1992.

7. Dong, Y, Forster, B C, and Ticehurst, C "Optimal decomposition of radar polarisation signatures," *IEEE Trans. on Geoscience and Remote Sensing*, vol. 36, no. 3, pp. 933-939, 1998.

8. Dong, Y, "L-band VV clutter analysis for natural land in Northern Territory areas," Research Report, DSTO-RR0254, DSTO, Australia, 2003.

9. Dong, Y, "Clutter spatial distribution and new approaches of parameter estimation for Weibull, and K- distributions," Research DSTO, Australia, 2004 (in publication).

10. Elachi, C, *Introduction to the Physics and Techniques of Remote Sensing*. New York: Wiley, 1987.

11. Helmken, H F, "Low grazing angle radar backscatter from the ocean surface," *IEE Proceedings, Part F*, vol. 137, no.2, pp. 113-117, 1990.

12. Horn, G, Milne, A K, and Finlayson, M, "Monitoring wetland inundation patterns using Radarsat multitemporal data," *Canadian Journal of Remote Sensing*, vol 26, no 2, pp. 133-137, April 2001.

13.Karam, M A, Fung, A. K, Lang, R H, and Chauhan, N S, "A microwave scattering model for layered vegetation," *IEEE Trans on Geoscience and Remote Sensing*, vol. 30, no. 4, pp. 767-784, July 1992.

14.Katzin, M, "On the mechanisms of radar sea clutter," Proceedings of IRE, vol. 45, pp. 44-54, 1957.

15.Kerr, D E (editor), *Propagation of Short Radio Waves*, MIT Radiation Laboratory Series, vol. 13, McGraw-Hill, 1951.

16.Lee, P H Y, Barter, J D, Hindman, C L, Lake, B M, and Rungaldier, H, "Angle and polarisation dependent microwave backscatter from ocean waves," *Proceedings of IGARSS' 94*, pp. 1272-1274, 8-12Aug 1994.

17.Long, M W (editor), *Airborne Early Warning System Concepts*, Artech House, 1992.

18.Long, M W, *Radar Reflectivity of Land and Sea*, 3rd Edition, Artech House, 2001.

19.Morchin, W C, *Airborne Early Warning Radar*, Artech House, 1990.

20.Nathanson, F E, Reilly, J P, and Cohen, M N, *Radar Design Principles*, 2nd Edition, Scitech Publishing Inc., 1999.

21.Rice, S O, "Reflection of electromagnetic waves from slightly rough surfaces," in *The Theory of Electromagnetic Waves*, M. Kline, Ed. New York: Wiley, 1951.

22.Richards, J A, Woodgate, P W, and Skidmore, A K, "An explanation of enhanced radar backscattering from flooded forests," *International Journal of Remote Sensing*, vol. 8, no. 7, pp. 1093-1100, 1987.

23.Ruck, G T, Barrick, D E, and Stuart, W D, *Radar Cross Section Handbook*, Plenum Press, 1970.

24.Skolnik, M I, *Introduction to Radar Systems*, 3rd edition, McGraw-Hill, 2001.

25.Trizna, D B, "A model for Brewster angle damping and multipath effects on the microwave radar sea echo at low grazing angles," *IEEE Trans on Geoscience and Remote Sensing*, vol. 35, no. 5, pp. 1232-1244, 1997.

26.Ulaby, F T, Moore, R K, and Fung, A K, *Microwave Remote Sensing: Active and Passive, Volume II: Radar Remote Sensing and Surface Scattering and Emission Theory*, Artech House, 1982.

27.Ulaby, F T, and Dobson, M C, *Handbook of Radar Scattering Statistics for Terrain*, Artech House, 1989.

28. Valenzuela, G R, "Depolarization of EM waves by slightly rough surfaces," *IEEE Trans. Antennas Propagation*, vol. AP-15, pp. 552–557, July 1967.

Appendix A: Surface Clutter at Low Grazing Angle Measured by Airborne Radar

The reported results for clutter at low grazing angle are often collected from surface radars (Billingsley, 2002, Long, 2001, Nathanson, 1999). Airborne MCARM (multi-channel airborne radar measurement) data are used to study the characteristics of clutter at low grazing angle in this report. The difference between surface radar data and airborne radar data lies in range distances. The height of a surface radar is usually within 50m with the radar horizon limiting clutter collection to 10 to 20 kilometres. On the other hand, the height of airborne radar is usually in hundreds to thousands of metres leading to the range in hundreds of kilometres to reach the horizon. It is not clear whether this significant difference in range results in different characteristics of clutter with respect to grazing angle.

In 1995-1996, the Air Force Research Laboratory, Rome Research Site collected MCARM data using a L-band VV polarised phased array radar. A BAC1-11 aircraft was used as the platform for the phased array antenna. Only the analogue sum channel data is used in this report.

One set of low PRF (PRF = 500) and one set of medium PRF (PRF = 1984) MCARM acquisition data are used in the study. Figure A-1 (a) shows aircraft positions and the main beam coverage of these two acquisitions over the DTE (digital terrain elevation) map of the region. An optical image of the area is also shown in Figure A-1 (b). Apart from bay water (Chesapeake Bay), the area can be best described as cultivated farmland with scattered trees. Man-built objects include highways/ freeways and sparsely distributed residential houses are also common. The terrain is relatively flat, and elevation in the radar's main beam areas is generally within 0-30 m. Since the radar's resolution of the analogue sum channel is very coarse (about $8\times10^5 m^2$), the landcover of the illuminated areas can only be categorised into two types, namely, farmland and bay water.

Data in range bins 1-200 are not used in analysis because there is a serious leakage of the transmitted signal in range bin 68, and also because we are more interested in low grazing angles. It is worth noting that all values shown are only relative values, because gains and losses in both RF and IF processing domains are unknown. Figure A-2 shows the received power with respect to range bins. The time interval between two consecutive range bins is $0.8\,\mu s$.

The grazing angle and depression angle with respect to range bin are shown in Figure A-3. In the calculation, the Earth was assumed to be a sphere with an effective radius of 4/3 times the real Earth radius (Long, 2001).

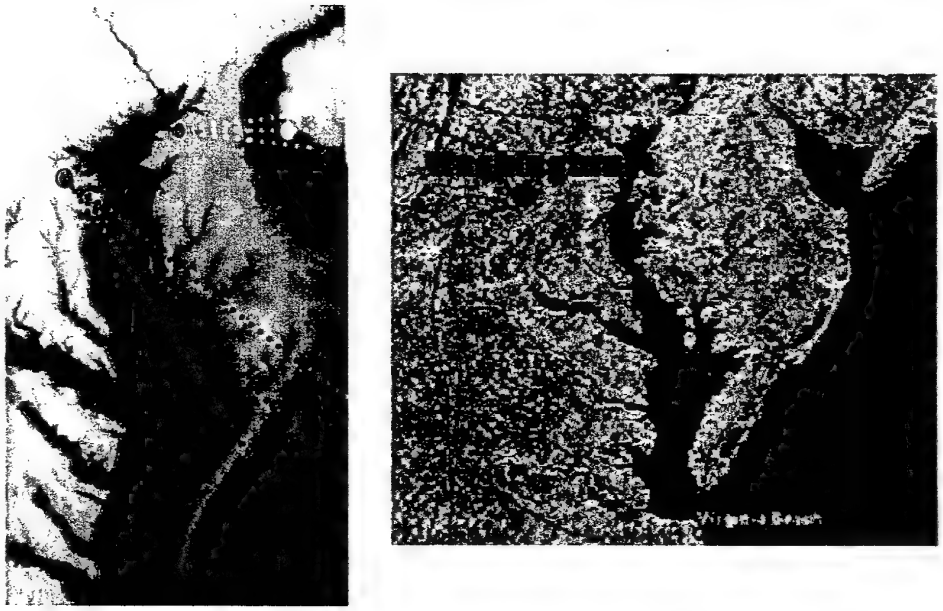

(a) (b)

Figure A-1: (a) Aircraft positions (the green dots) of the low and medium PRF acquisitions overlay to the DTE map of the region. The coverage of the main beam of the radar is also shown. The red dots are for the low PRF acquisition, representing range bins 500, 1000 and 1500, respectively. The yellow dot is for the medium PRF acquisition, representing a range bin 450. The time interval of range bins is 0.8 μs. (b) An optical image of the region.

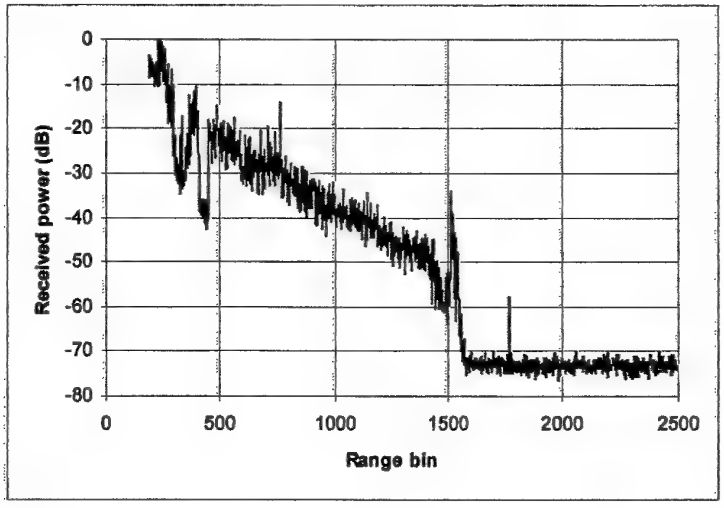

Figure A-2: Received power of the low PRF acquisition.

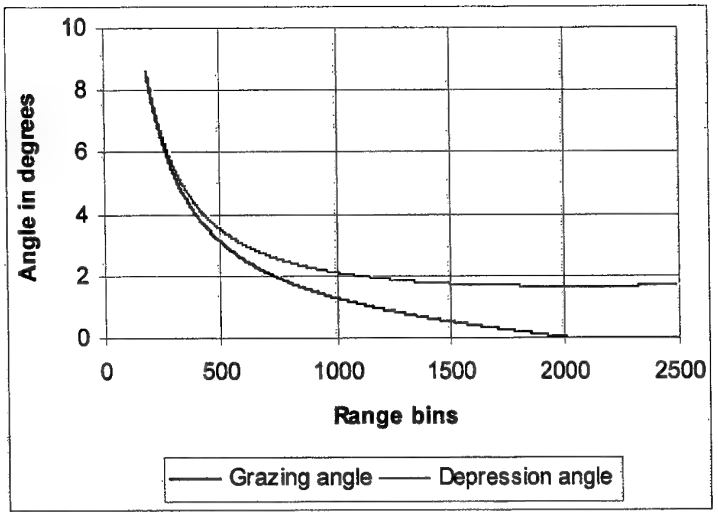

Figure A-3: Grazing angle and depression angle with respect to range bins of the low PRF acquisition.

It can be seen that the received power is down to the noise level before the grazing angle approaches zero degrees. This might be due to the effect of multipath propagation. We should also notice that the A/D conversion used is 14 bits, which gives a dynamic range of 78dB. The dynamic range shown in Figure A-2 is about 70dB, and possible another 10dB in bins 1-200. It seems therefore that in general more than 14bits are required to cover the dynamic range of low PRF clutter.

Now let us work out the dependence of clutter on grazing angle. Assuming the clutter coefficient in the 3dB main beamwidth area to be constant, according to (1) and (2) we have,

$$P_{r3dB} \propto \frac{\sigma_0 F^4}{R^3} \int_{\phi_{3dB}} G_t(\alpha,\phi) G_r(\alpha,\phi) d\phi \qquad \text{(A-1)}$$

where P_{r3dB} is the power received from the area illuminated by the main beam beamwidth. For a radar looking broadside to the direction of flight, the isodops are orthogonal to the range rings. Therefore, after the received power is transformed into the frequency domain, the corresponding component of P_{r3dB} can be determined accordingly. We write,

$$P_{r3dB} = \sum_{f=f_1}^{f_2} P(f) \qquad \text{(A-2)}$$

where $P(f)$ is the power component of the frequency f and

$$f_1 = \frac{2v}{\lambda}\cos\alpha\cos\left(\frac{\pi}{2}+\frac{\phi_{3dB}}{2}-\delta_0\right) \tag{A-3}$$

$$f_2 = \frac{2v}{\lambda}\cos\alpha\cos\left(\frac{\pi}{2}-\frac{\phi_{3dB}}{2}-\delta_0\right) \tag{A-4}$$

where v is the velocity of the platform, α the depression angle, δ_0 the drift angle of the platform and ϕ_{3dB} the azimuth angle of 3dB beamwidth.

We then have the final expression for the dependence of clutter on depression angle (the corresponding grazing angle can be calculated),

$$\sigma_0 F^4 \propto \frac{P_{r3dB}R^3}{G^2(\alpha)} \tag{A-5}$$

where

$$G^2(\alpha) = \int_{\phi_{3dB}} G_t(\alpha,\phi)G_r(\alpha,\phi)d\phi \tag{A-6}$$

The above integration is along the contour of constant-elevation, which also assumes the range on the contour of constant-elevation is the same. Rigorously speaking, the contour of constant elevation angle of a tilt antenna array on the ground is nearly a straight line whereas the contour of the equal-range is a circle. However, we can consider the two contours to be coincident for a small angle of ϕ_{3B}.

Figure A-4 shows the power distribution in range-Doppler bins for the low PRF acquisition. It can be seen that the Doppler frequency at the boresight is not zero due to the drift of the aircraft. The dependence of clutter on grazing angle is shown in Figure A-5. If we ignore those obvious point targets, the difference between clutter of farmland and clutter of bay water is distinct.

The dependence of clutter on grazing angle calculated from the medium PRF is also shown in Figure A-5. The trend of the pattern seems consistent with the clutter pattern obtained from low PRF acquisitions for both farmland and bay water.

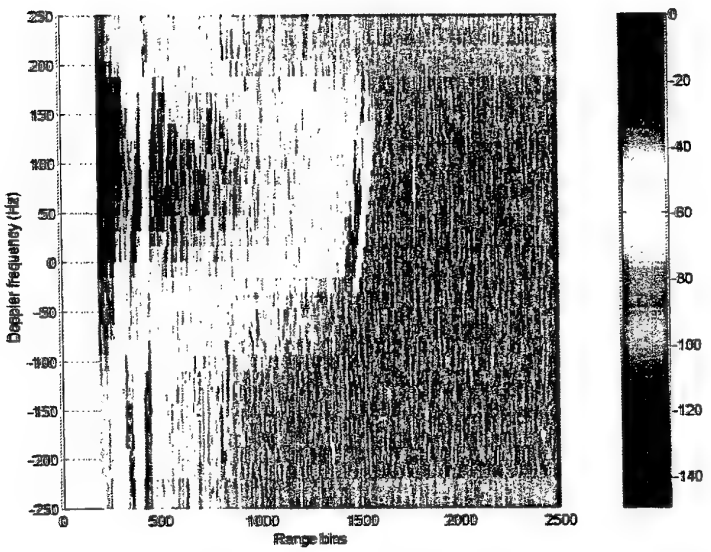

Figure A-4: Power distribution in range-Doppler bins of the Low PRF acquisition. Due to the drift, the Doppler frequency at the boresight is not zero.

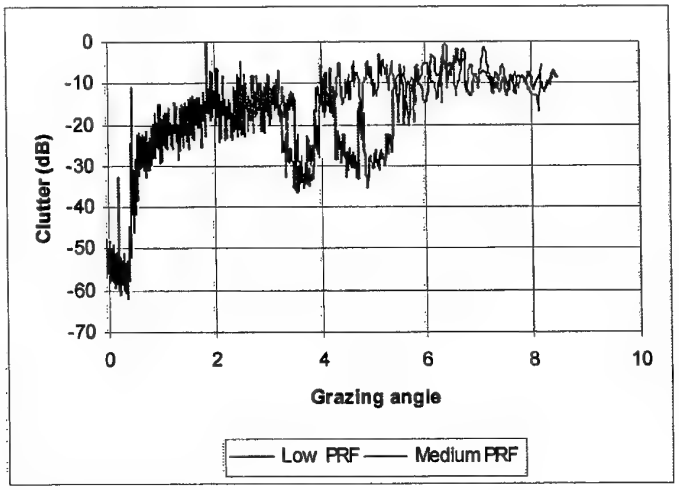

Figure A-5: The clutter pattern obtained from a low PRF acquisition (acquisition 55) consists with clutter pattern obtained from a medium PRF acquisition (acquisition 575) for both farmland and bay water.

It should also be pointed out that Figure A-5 shows an apparent increase in clutter with a decrease in grazing angle close to zero degrees. The original received signal was masked by the radar's noise floor, as shown in Figure A-2. The process of noise is still noise. This increasing pattern simply reflects the process of cancellation of the range effect over the flat noise.

Appendix B: Backscattering Coefficient of a Flat Conducting Surface of Infinite Extent at Normal Incidence[10]

The radar cross section (RCS), σ, of a flat conducting surface of infinite extent at normal incidence may be determined by the use of the image theory as shown in Figure B1. According to the definition of the RCS,

$$\sigma = \lim_{R\to\infty} 4\pi R^2 \frac{S_s}{S_i} \tag{B1}$$

where S_s and S_i are the scattered and incidence power densities, respectively, as

$$S_i = \frac{P_T G}{4\pi R^2} \tag{B2}$$

$$S_s = \frac{P_T G}{4\pi (2R)^2} \tag{B3}$$

where P_T is the radar's transmitted power, G the antenna gain and R the range.

Inserting (B2) and (B3) to (B1), we have

$$\sigma = \pi R^2 \tag{B4}$$

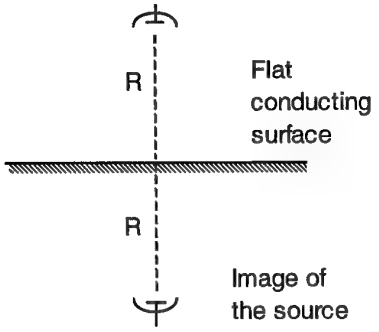

Figure B1: Using the image theory to determine the scattered power density.

[10] The derivation of the appendix follows a path suggested by Dr John Whitrow.

Equation (B4) may be interpreted as following. The power intercepted by the surface is $\frac{P_T G}{4\pi R^2}\cdot\sigma$, which when scattered isotropically (times a factor of $\frac{1}{4\pi R^2}$) produces at the receiver a power density of $\frac{P_T G}{4\pi(2R)^2}$, according to the image theory. That is,

$$\frac{P_T G}{4\pi R^2}\cdot\sigma\cdot\frac{1}{4\pi R^2}=\frac{P_T G}{4\pi(2R)^2} \tag{B5}$$

Reorganising (B5) gives (B4).

Assuming that the antenna gain of the illuminated areas is G, and zero otherwise, we have the following identity,

$$A_i G = 4\pi R^2 \tag{B6}$$

where A_i is the illuminated area.

The backscattering coefficient, by the definition is then,

$$\sigma_0 = \frac{\sigma}{A_i} = \frac{G}{4} \tag{B7}$$

Therefore, the backscattering coefficient of a flat conducting surface of infinite extent at normal incidence is dependent on the gain, or equivalently, on the beamwidth.

DISTRIBUTION LIST

Models of Land Clutter vs Grazing Angle, Spatial Distribution and Temporal Distribution — L-band VV Polarisation Perspective

Yunhan Dong

AUSTRALIA

DEFENCE ORGANISATION		**No. of copies**
Task Sponsor		
OCAEWCSPO		1
S&T Program		
Chief Defence Scientist FAS Science Policy AS Science Corporate Management Director General Science Policy Development	shared copy	1
Counsellor Defence Science, London		Doc Data Sheet
Counsellor Defence Science, Washington		Doc Data Sheet
Scientific Adviser to MRDC, Thailand		Doc Data Sheet
Scientific Adviser Joint		1
Navy Scientific Adviser		Doc Data Sht & Dist List
Scientific Adviser - Army		Doc Data Sht & Dist List
Air Force Scientific Adviser		1
Scientific Adviser to the DMO M&A		1
Scientific Adviser to the DMO ELL		Doc Data Sht & Dist List
Director of Trials		1
Systems Sciences Laboratory		
Chief of Electronic Warfare and Radar Division		Doc Data Sht & Dist List
Research Leader Microwave Radar		Doc Data Sht & Dist List
Head RST, EWRD: Dr J Whitrow		1
Task Manager: Mr G Lawrie		1
Head IRS, ISRD: Dr N Stacy		1
Head RFS, WSD: Dr A Szabo		1
Mr S Capon, RST Group, EWRD		1
Dr L Powis, RST Group, EWRD		1
Mr J Baldwinson, RMA Group, ERWD		1
Author: Dr Y Dong		1
EWSTIS		(PDF Format) 1
DSTO Library and Archives		
Library Edinburgh		1
Australian Archives		1

Capability Systems Division

Director General Maritime Development	Doc Data Sheet
Director General Aerospace Development	Doc Data Sheet
Director General Information Capability Development	Doc Data Sheet

Office of the Chief Information Officer

Deputy CIO	Doc Data Sheet
Director General Information Policy and Plans	Doc Data Sheet
AS Information Structures and Futures	Doc Data Sheet
AS Information Architecture and Management	Doc Data Sheet
Director General Australian Defence Simulation Office	Doc Data Sheet

Strategy Group

Director General Military Strategy	Doc Data Sheet
Director General Preparedness	Doc Data Sheet

HQAST

SO (Science) (ASJIC)	Doc Data Sheet

Navy

Director General Navy Capability, Performance and Plans, Navy Headquarters
Doc Data Sheet

Director General Navy Strategic Policy and Futures, Navy Headquarters
Doc Data Sheet

Army

ABCA National Standardisation Officer, Land Warfare Development Sector, Puckapunyal
e-mailed Doc Data Sheet

SO (Science), Deployable Joint Force Headquarters (DJFHQ) (L), Enoggera QLD
Doc Data Sheet

SO (Science) - Land Headquarters (LHQ), Victoria Barracks NSW
Doc Data & Exec Summ

Intelligence Program

DGSTA Defence Intelligence Organisation	1
Manager, Information Centre, Defence Intelligence Organisation	1

Assistant Secretary Corporate, Defence Imagery and Geospatial Organisation
Doc Data Sheet

Defence Materiel Organisation

Head Airborne Surveillance and Control	Doc Data Sheet
Head Aerospace Systems Division	Doc Data Sheet
Head Electronic Systems Division	Doc Data Sheet
Head Maritime Systems Division	Doc Data Sheet
Head Land Systems Division	Doc Data Sheet
Head Industry Division	Doc Data Sheet
Chief Joint Logistics Command	Doc Data Sheet
Management Information Systems Division	Doc Data Sheet
Head Materiel Finance	Doc Data Sheet

Defence Libraries

Library Manager, DLS-Canberra	Doc Data Sheet
Library Manager, DLS - Sydney West	Doc Data Sheet

OTHER ORGANISATIONS

National Library of Australia	1
NASA (Canberra)	1

UNIVERSITIES AND COLLEGES

Australian Defence Force Academy	
Library	1
Head of Aerospace and Mechanical Engineering	1
Serials Section (M list), Deakin University Library, Geelong, VIC	1
Hargrave Library, Monash University	Doc Data Sheet
Librarian, Flinders University	1

OUTSIDE AUSTRALIA

INTERNATIONAL DEFENCE INFORMATION CENTRES

US Defense Technical Information Center	2
UK Defence Research Information Centre	2
Canada Defence Scientific Information Service	1
NZ Defence Information Centre	1

ABSTRACTING AND INFORMATION ORGANISATIONS

Library, Chemical Abstracts Reference Service	1
Engineering Societies Library, US	1
Materials Information, Cambridge Scientific Abstracts, US	1
Documents Librarian, The Center for Research Libraries, US	1

INFORMATION EXCHANGE AGREEMENT PARTNERS

National Aerospace Laboratory, Japan	1
National Aerospace Laboratory, Netherlands	1

AFRL, Rome, NY: Dr M Davis	1
SPARES	5
Total number of copies:	**43**

Page classification: UNCLASSIFIED

DEFENCE SCIENCE AND TECHNOLOGY ORGANISATION DOCUMENT CONTROL DATA					1. PRIVACY MARKING/CAVEAT (OF DOCUMENT)
2. TITLE Models of Land Clutter vs Grazing Angle, Spatial Distribution and Temporal Distribution – L-Band VV Polarisation Perspective					3. SECURITY CLASSIFICATION (FOR UNCLASSIFIED REPORTS THAT ARE LIMITED RELEASE USE (L) NEXT TO DOCUMENT CLASSIFICATION) Document (U) Title (U) Abstract (U)
4. AUTHOR(S) Yunhan Dong					5. CORPORATE AUTHOR Systems Sciences Laboratory PO Box 1500 Edinburgh SA 5111
6a. DSTO NUMBER DSTO-RR-0273	6b. AR NUMBER AR-013-074		6c. TYPE OF REPORT Research Report		7. DOCUMENT DATE March 2004
8. FILE NUMBER 2004/1017735/1	9. TASK NUMBER AIR02/232	10. TASK SPONSOR OCAEWCSPO	11. NO. OF PAGES 74	12. NO. OF REFERENCES 28	
13. URL on the World Wide Web http://www.dsto.defence.gov.au/corporate/reports/DSTO-RR-0273.pdf			14. RELEASE AUTHORITY Chief, Electronic Warfare and Radar Division		
15. SECONDARY RELEASE STATEMENT OF THIS DOCUMENT Approved for Public Release OVERSEAS ENQUIRIES OUTSIDE STATED LIMITATIONS SHOULD BE REFERRED TO DOCUMENT EXCHANGE, PO BOX 1500, EDINBURGH, SA 5111, AUSTRALIA					
16. DELIBERATE ANNOUNCEMENT No Limitations					
17. CASUAL ANNOUNCEMENT Yes					
18. DEFTEST DESCRIPTORS Ground clutter Distribution Scattering Grazing angle					

19. ABSTRACT

Land clutter issues and modelling from a perspective of L-band VV polarisation are addressed. In particular, clutter distributions in three different dimensions are discussed in detail. First a three-term model for the dependence of land clutter on grazing angle is proposed. The model is site-specific and landcover-dependent. Parameters for dominant types of landcover in the Northern Territory region are regressed using AirSAR and MCARM measurements as well as others available in literature. Clutter spatial distribution is also investigated. Aimed at real-time implementation, a simple and fast parameter estimation scheme for the Weibull and K- distributions is given. The estimates are found to be nearly identical to the maximum likelihood estimates. Discussed finally in the report is the clutter temporal distribution (Doppler spectrum) due to motion of moving parts of scatterers. Billingsley's exponential decay modelis summarised.